Taylor, K. W. R., Willumsen, P. S., Hollis, C. J., & Pancost, R. (2018). South Pacific evidence for the long-term climate impact of the Cretaceous/Paleogene boundary event. *Earth-Science Reviews*, *179*, 287-302. https://doi.org/10.1016/j.earscirev.2018.02.012

South Pacific evidence for the long-term climate impact of the Cretaceous/Paleogene boundary event

Kyle W.R. Taylor[a,b], Pi Suhr Willumsen[c], Christopher J. Hollis[d], Richard D. Pancost[a]

[a]Organic Geochemistry Unit, The Cabot Institute and School of Chemistry, University of Bristol, Cantock's Close, Bristol BS8 1TS, UK

[b]Elementar UK Limited, Isoprime House, Earl Road, Cheadle Hulme, Cheadle, Sk8 6PT, UK

[c]Department of Geoscience, Aarhus University, Høegh-Guldbergs Gade 2, 8000 Aarhus C, Denmark

[d]GNS Science, P.O. Box 30-368, Lower Hutt, New Zealand

Abstract

The Cretaceous/Paleogene (K/Pg) boundary is well-represented across a range of depositional settings in New Zealand. Trends in fossil assemblages and marine lithofacies indicate that the K/Pg event was followed by a pronounced and long-term (~1 Myr) perturbation in climate and ocean conditions. These findings are supported by a TEX_{86}-derived sea surface temperature (SST) reconstruction across the K/Pg boundary at mid-Waipara River, north Canterbury. The BAYSPAR calibration indicates that SST was very stable in the uppermost Cretaceous (~20°C), but abruptly warmed by ~4°C in a 25 cm-thick lowermost Paleocene interval. This interval is overlain by a ~2 m thick interval in which SST abruptly cooled by ~10°C and then progressively returned to ~20°C. The basal Paleocene warm interval is associated with an acme in the dinoflagellate species *Trithyrodinium evittii* and the succeeding cool interval is associated with an acme in *Palaeoperidinium pyrophorum*. Biostratigraphic correlation of the shelfal mid-Waipara section to the pelagic K/Pg sections in Marlborough reveals that a significant unconformity separates these two acme events, with the T acme event occurring in the earliest Paleocene and the *P. pyrophorum* acme occurring ~1 Myr later and lasting ~200 kyr. A succession of dinoflagellate

acme events within the intervening interval in the Marlborough sections implies unstable climatic and environmental conditions in the lead up to the *P. pyrophorum* acme and cooling event at ~65 Ma. This event also coincides with a peak in biogenic silica accumulation in the Marlborough sections. We suggest that disruption to biogeochemical pathways at the K/Pg boundary caused long-term climatic cooling in the southern Pacific region.

Keywords:

TEX_{86}, Cretaceous-Paleogene Boundary, Paleoclimate, Paleoceanography, Geochemistry, Palynology, Organic Geochemistry, Biostratigraphy, New Zealand, Southwest Pacific

1. Introduction

The long-term consequences of the Cretaceous–Paleogene (K/Pg) boundary event on Earth's climate remain poorly understood. Numerical models simulating the effects of the K/Pg boundary impact predict a brief (years to decades) period of global cooling induced by sulphate aerosols and dust or soot blocking out the sun's radiation, the so-called 'impact winter' (Pope et al., 1994, 1997; Pierazzo et al., 2003; Schulte et al., 2010; Bardeen et al. 2017; Brugger et al. 2017), followed by a longer episode of global warmth likely caused by both CO_2 released by the impact and reduced CO_2 uptake by plants (Pierazzo et al., 1998; Kring, 2007). This pattern of short-lived cooling followed by longer-term warming is supported by microfossil evidence in Northern Hemisphere sites (Brinkhuis et al., 1998; Galeotti et al., 2004), and has been corroborated by integrated study of the TEX_{86} sea surface temperature (SST) proxy and dinoflagellate assemblages (Vellekoop et al., 2014). TEX_{86}-based temperature reconstructions from other regions (Kemp et al., 2014; Vellekoop et al., 2015; 2016; Petersen et al., 2016) provide further evidence for SST change following the K/Pg boundary. There is also some evidence that Deccan Traps volcanism affected

53 climate through the K–Pg transition (Courtillot et al., 1988; Chenet et al., 1988; Self et al.,
54 2014; Schoene et al., 2015; Petersen et al., 2016).

55 Longer-term climate impacts of the K/Pg event have been inferred from stable oxygen
56 isotope records. However, poor preservation and the K/Pg extinction of planktic calcifying
57 organisms (Zachos and Arthur, 1986; Magaritz et al., 1992) makes interpretation difficult.
58 Ocean warming has been inferred in some studies (e.g. Douglas and Savin, 1971;
59 Oberhänsli, 1986; Barrera and Keller, 1990; Stott and Kennett, 1990; Schmitz et al., 1992;
60 Barrera and Keller, 1994), whereas others suggest cooling (Boersma and Shackleton, 1977;
61 Boersma et al., 1979; 1981; Keller and Lindinger, 1989) or no significant change at all
62 (Zachos and Arthur, 1986). Other studies have inferred climate fluctuations over the first 1-2
63 Myrs of the Paleocene from indirect evidence, such as oscillations in magnetic susceptibility,
64 carbonate content and grain size (D'Hondt et al., 1996; Kroon et al., 2007).

65 For the southwest Pacific, a pattern of short-lived climate instability followed by prolonged
66 climatic cooling over ~1 Myrs has been inferred from both marine and terrestrial K/Pg
67 boundary records (Vajda et al., 2001; Hollis, 2003; Vajda and Raine, 2003). Prolonged
68 cooling has been invoked to explain both a delayed recovery of calcareous plankton and the
69 abundance of diatoms and radiolarians in the basal Paleocene pelagic sediments of
70 northeastern South Island, New Zealand (Hollis et al., 1995, 2003a, b). Compositional shifts
71 in the marine dinoflagellate cyst assemblages have been interpreted as alternating periods
72 of warm and cool SSTs (Willumsen & Vajda, 2010b). However, these climate fluctuations
73 have been inferred from changes in fossil assemblages or lithology and lack corroboration
74 from geochemical proxies for temperature. In this study, we use the TEX_{86} proxy to
75 reconstruct SST across the K/Pg boundary in the mid-Waipara section, Canterbury Basin
76 (Fig. 1). We combine previously reported data for the early Paleocene (Taylor et al., 2013)
77 with new analyses from the uppermost Cretaceous. We also evaluate different GDGT
78 paleothermometers and consider how changes in thaumarchaeotal growth environment
79 might be reflected in this record.

The mid-Waipara River section (Fig. 1) contains the most complete known K/Pg transition in a neritic setting in the South Pacific region (Hollis and Strong, 2003). It provides an important link between bathyal marine and terrestrial sections in New Zealand (Hollis, 2003) and is one of only two neritic K/Pg boundary record in the Southern Hemisphere, the other being on Seymour Island, Antarctic Peninsula (Elliot et al., 1994; Bowman et al., 2012; 2014; 2015; Kemp et al., 2014; Petersen et al., 2016; Witts et al., 2016). The mid-Waipara section contains abundant and diverse palynomorphs, including dinoflagellates (Wilson, 1987; Willumsen, 2004; 2006; 2012; Ferrow et al., 2011) and terrestrial palynomorphs (Vadja et al., 2001; Vadja and Raine, 2003; Ferrow et al., 2011), which provide qualitative indications of climatic and environmental variability. Importantly, the dinoflagellate succession can be correlated to two bathyal K/Pg boundary sections in eastern Marlborough, Branch and Mead Streams (Fig. 1), utilising a new Paleocene dinoflagellate zonation (Crouch et al., 2014) and a well-defined succession of early Paleocene acme events (Willumsen, 2004, 2006, 2011; Willumsen & Vajda, 2010b). Collectively, these data allow us to reconstruct climatic and oceanic changes through the K/Pg boundary transition in the mid-latitude southwest Pacific.

2. Materials and Methods

2.1. Location and samples

The Waipara River trends northwest-southeast through a Mesozoic-Cenozoic sedimentary succession in northern Canterbury (Fig. 1).

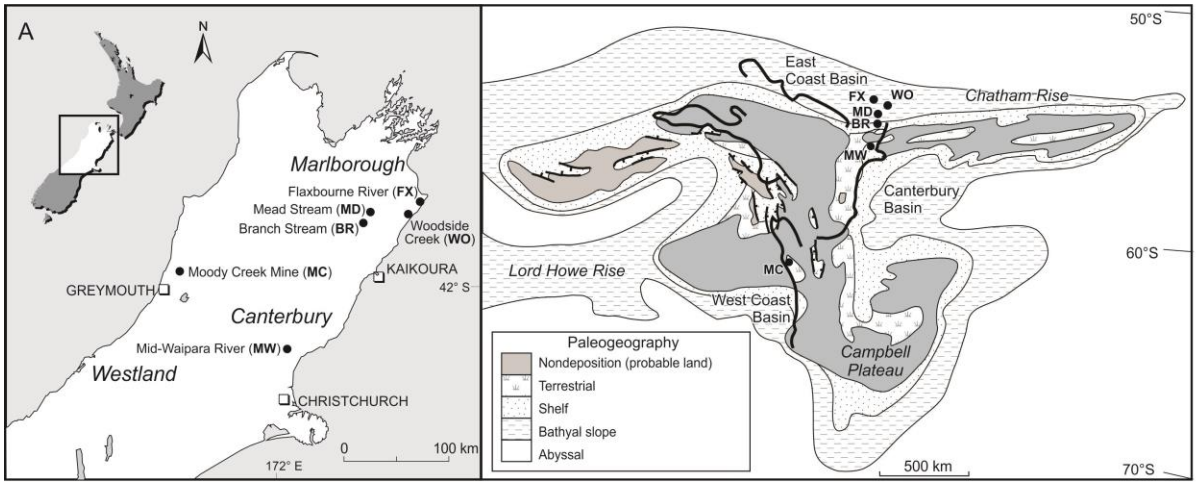

Figure 1. Location of the mid-Waipara River section and other Cretaceous-Paleogene (K/Pg) boundary sections discussed in the text: (A) present day location and (B) earliest Paleocene paleogeographic setting (adapted from Hollis et al., 2003a).

The section examined is referred to as the mid-Waipara River section because it is located along the middle course of the river. The K/Pg boundary is located within Column 1 in the composite section described by Morgans et al. (2005). It lies at the base of a 4-m thick, non-calcareous, glauconitic sandstone, which forms the uppermost unit of the Conway Formation (Fig. 2). The underlying Conway Formation is moderately calcareous and more mud-rich. Overlying the Conway Formation is the lower Paleocene Loburn Formation, a ~60 m-thick unit of non-calcareous to slightly calcareous sandy mudstone. These sediments were deposited in a neritic mid-shelf setting during a widespread marine transgression (Field et al., 1989).

Geochemical studies (Brooks et al., 1986; Hollis and Strong, 2003; Ferrow et al., 2011) place the boundary within an irregular 2-cm thick, 'rusty' Fe-stained interval that includes a relatively small Ir anomaly (0.49 ng/g, ~50 x crustal average) as well as enrichment in Fe, Ni, Zn and Cr (Fig. 2). As discussed by Hollis and Strong (2003), an irregular distribution of these elements is probably due to intense bioturbation in these sediments (See S1 for cross-plotted trace metal concentrations)

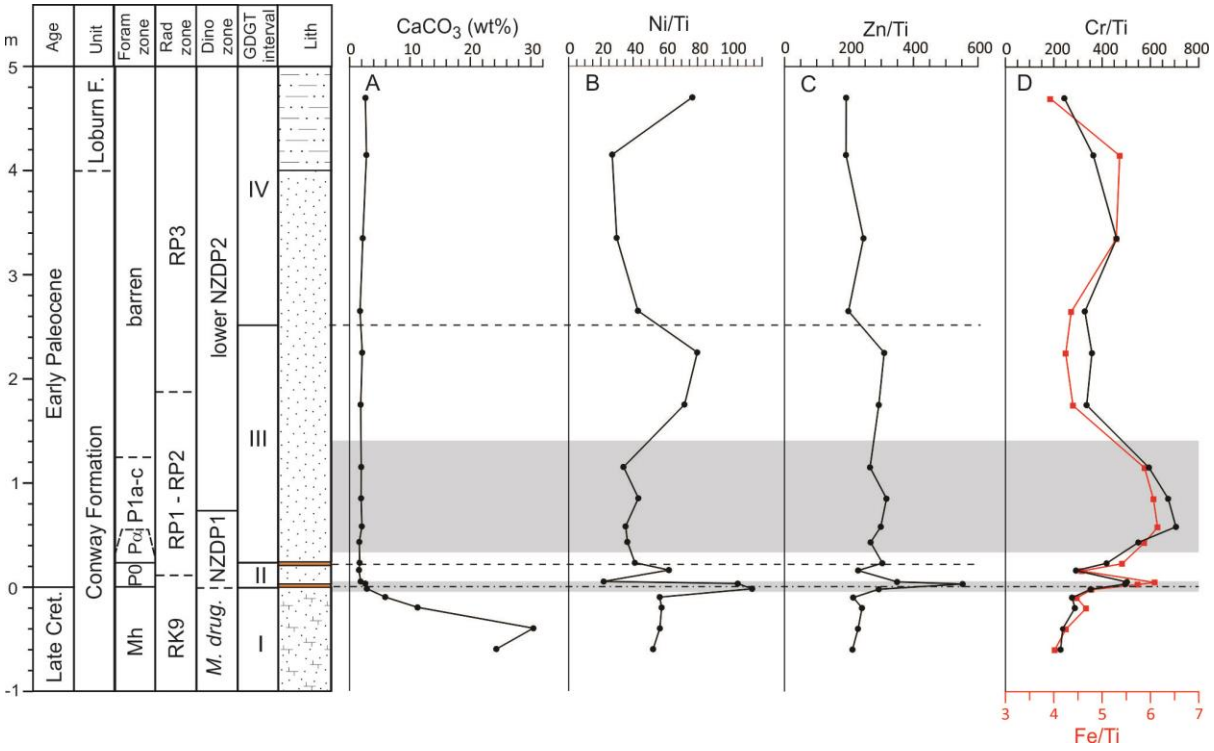

Figure 2. Stratigraphy and geochemical profiles for the uppermost Cretaceous and lower Paleocene succession at mid-Waipara River. Foraminiferal and radiolarian datums are from Hollis and Strong (2003). Dinoflagellate datums are from Willumsen (2004, 2011, 2012) and Crouch et al. (2014). Geochemical profiles include calcium carbonate concentration (A) and concentrations of Ni (B), Zn (C), Cr and Fe (D) normalised to Ti to account for terrigenous sources.

Willumsen (2006) and Ferrow et al. (2011) also noted downward displacement and mixing of dinoflagellate cyst assemblages. A prominent dark, irregular band in the middle of this zone is chosen as the stratigraphic position of the K/Pg boundary (zero datum) but elemental anomalies suggest boundary components have been mixed by bioturbation into sediments 5 cm above and below this datum (Fig. 2A-D). The boundary also coincides with a marked decrease in $CaCO_3$ concentration (Fig. 2A) from ~30 wt% in the Cretaceous to <5 wt% over the lower 5 m of Paleocene strata (Hollis and Strong, 2003). In contrast to the sudden

decrease recorded in the bathyal Marlborough sections (Hollis et al., 2003a; b), $CaCO_3$ concentration begins to decrease c. 0.3 m below the boundary, also likely due to bioturbation. A second “rusty” zone ~20-22 cm above the K/Pg boundary is also associated with Fe and Cr enrichments that extend to at least 1.2 m above the boundary (Fig. 2). The combined enrichment of these elements over an extended interval may indicate dysoxic conditions (Calvert and Pedersen, 1993).

Our TEX_{86} study is based on 26 samples that extend from 1.15 m below to 20 m above the K/Pg boundary, including a suite of 15 closely spaced samples that span the boundary (Supplementary materials S2). The same sample set was utilised for earlier geochemical, micropaleontological, palynological and geochemical studies of this section (Hollis and Strong, 2003; Vajda and Raine, 2003; Willumsen, 2006; 2012; Crouch et al., 2014). In Ferrow et al. (2011), a new sample suite of 17 samples from a slabbed section through the mid-Waipara River K/Pg boundary interval, from 0.24 m below to 0.26 m above the boundary, was examined for Mössbauer spectroscopy, mineralogy, osmium isotopes, dinoflagellate cysts, spores and pollen. These samples are not utilised in the present study because they do not provide a longer term record of environmental change and are difficult the correlate confidently with the previously collected sample suite.

2.2. Biostratigraphy and palynology

Despite the scarcity of calcareous microfossils and radiolarians in the mid-Waipara section, Hollis and Strong (2003) were able to identify planktic foraminiferal zones P0, Pα and P1a-c and radiolarian zones RP1 to RP3. In contrast, dinoflagellates are abundant and well-preserved throughout the section (Wilson, 1987; Willumsen, 2004; 2006, 2012) and dinoflagellate biostratigraphy provides the primary age control and to correlate with the bathyal sections in Marlborough (Willumsen, 2011; Crouch et al., 2014), complemented by planktic foraminiferal and radiolarian bioevents (Fig. 2). Processing methods for

161 micropaleontology and palynology are described elsewhere (Hollis and Strong, 2003; Vajda
162 and Raine, 2003; Willumsen, 2003; 2004; 2006; 2011; 2012). Dinoflagellate census data are
163 based on counts of ~300 specimens (Willumsen, 2003). Data for selected taxa from the
164 uppermost Cretaceous and lower 5 m of Paleocene strata at mid-Waipara have been
165 previously reported by Willumsen (2004; 2006; 2012). Data for additional taxa from this
166 interval and an additional 5 samples from the overlying Paleocene interval are from
167 Willumsen (2003). Data for the basal 9 samples from the Loburn Formation in mid-Waipara
168 Column 4 (Morgans et al., 2005) are from Crouch et al. (2014). Data for Columns 1 and 4
169 sets are combined by approximate correlation of the top of column 1 with the base of column
170 4, which is consistent with the dinoflagellate biostratigraphy (Supplementary materials S3)
171 although a small overlap between the two sections is possible. Dinoflagellate census data for
172 the Mead and Branch sections were reported by Willumsen (2003; 2011).

173

174 *2.3. Glycerol Dialkyl Glycerol Tetraether (GDGT) analysis, calibration and indices*

175

176 Glycerol dialkyl glycerol tetreathers (GDGTs) were extracted from sediments and analysed
177 by liquid chromatography mass spectrometer (LC-MS) as per methods described in the
178 supplementary information in Taylor et al. (2013) (Supplementary materials S4).

179

180 The original TEX_{86} core-top calibration to SST was linear (Schouten et al., 2002; Kim et al.,
181 2008), with two complementary logarithmic indices introduced by Kim *et al.* (2010). TEX_{86}^{H}
182 was recommended for use in sites or sections where SST is expected to be greater than
183 15°C and TEX_{86}^{L} was recommend for sites where SST is expected to span 15°C. TEX_{86}^{H}
184 utilises the same combination of GDGTs as in the original linear TEX_{86} relationship
185 (Schouten et al., 2002; Kim et al., 2008):

186

187 $$TEX_{86} = (GDGT\text{-}2 + GDGT\text{-}3 + cren')/ (GDGT\text{-}1+ GDGT\text{-}2 + GDGT\text{-}3 + cren')$$

where for GDGT-n, *n* denotes the number of cyclopentyl moieties present and cren' denotes the crenarchaeol region-isomer (4 cyclopentyl rings, plus the cyclohexyl moiety).See Schouten et al. (2012) for GDGT structures as per this nomenclature. However TEX_{86}^{H}, when described as an index (rather than when referring to calibration-derived SST – see below), specifically refers to the logarithmic transformation of the original TEX_{8}:

$$TEX_{86}^{H} = \log TEX_{86}$$

TEX_{86}^{L} comprises a combination of GDGTs that is different from TEX_{86}^{H} and all other TEX_{86} equations, and is again a logarithmic transformation of the ratio of certain GDGTs:

$$TEX_{86}^{L} = \log \text{GDGT-2}/(\text{GDGT-1} + \text{GDGT-2} + \text{GDGT-3})$$

The TEX_{86}^{H} and TEX_{86}^{L} indices are subsequently used to derive SST (in degrees Celsius) using the following equations:

TEX_{86} [linear]: $SST = 81.5 \times TEX_{86} - 26.6$ (calibration error, ±5.2°C)

TEX_{86}^{H}: $SST = 68.4 \times \log TEX_{86} + 38.6$ (calibration error, ±2.5°C)

TEX_{86}^{L}: $SST = 67.5 \times \log TEX_{86}^{L} + 46.9$ (calibration error, ±4°C)

The TEX_{86} [linear] and TEX_{86}^{H} calibrations are based on modern core-top data from only settings where SST >15°C, whereas TEX_{86}^{L} is based on the entire global core-top sediment dataset (Kim et al., 2010). Recent papers (Taylor et al., 2013; Hernandez-Sanchez et al., 2014; Inglis et al., 2015) have noted that the TEX_{86}^{L} calibration yields spurious SST values under certain conditions where unusual variations in GDGT distributions occur .

A fourth core-top calibration, BAYSPAR, is a spatially-varying, Bayesian regression model for TEX_{86} that assumes a linear relationship between TEX_{86} and SST (Tierney and Tingley, 2015). For pre-Quaternary studies, a 'Deeptime' approach is recommended in which Bayesian statistics is used to identify the modern core-top samples that are closest to the measured TEX_{86} value and a linear regression is applied to these modern locations. Temperatures are calculated using www.whoi.edu/bayspar and can be reported as surface ($BAYSPAR_{SST}$) or subsurface ($BAYSPAR_{SubT}$) temperature; the latter is the weighted average of the temperature range over 0–200 m water depth.

GDGT distributions in suspended particulate material (SPM) have also been calibrated to *in situ* weighted-average water temperatures over a depth range of 0–100 m (Schouten et al., 2013).

SPM-TEX_{86}: Temperature (°C) = 59.6 x TEX_{86}^{H} + 32 (r^2 = 0.78, n = 88)

As expected, this equation yields temperatures similar to the depth-integrated 0–200 m TEX_{86}^{H} calibration and the $BAYSPAR_{SubT}$ calibration.

To examine further the applicability of the TEX_{86} paleothermometer in the Paleogene, Hollis et al. (2012) compiled data from four Paleogene studies (Zachos et al., 2006; Pearson et al., 2007; Burgess et al., 2008; Hollis et al., 2009) in which a representative range of TEX_{86} values could be compared to SST estimates derived from $\delta^{18}O$ values or Mg/Ca ratios in well-preserved, mixed-layer planktic foraminifera from the same samples. A strong correlation was observed between TEX_{86} values with SSTs derived from these inorganic proxies, but SSTs calculated with the TEX_{86}^{H} calibration were typically 3 to 6°C higher than foraminifera-based SSTs. Hollis et al. (2012) used a logarithmic regression to derive a paleo-calibration to SST ($pTEX_{86}$):

241 $pTEX_{86}$: SST = 39.036 x ln(TEX_{86}) + 36.455 (r^2 = 0.87, n = 42)

242

243 The $pTEX_{86}$ approach assumes that SST derived from well-preserved foraminiferal calcite
244 has greater fidelity in the Paleogene than TEX_{86} calibrations based on modern sediments.
245 The reasons for the offset between TEX_{86} and foraminiferal proxies for SSTS have been
246 widely discussed but with no consensus reached (Taylor et al., 2013; Inglis et al., 2015; Ho
247 and Laepple, 2016; Zhang et al., 2016). The issue has not been resolved with the
248 introduction of the BAYSPAR calibration, which results in an offset similar to that observed
249 for TEX_{86}^{H}.

250

251 A further way that GDGT distributions have been related to temperature is by calculating the
252 isoprenoidal GDGT 'degree of cyclisation', or $Ring_{AV}$ (e.g. Shimada et al., 2002, Schouten et
253 al., 2007, Pearson et al., 2008, Pitcher et al., 2009):

254

255 $Ring_{AV}$ = (1 x GDGT-1) + (2 x GDGT-2) + (3 x GDGT-3) + (4 x cren') / (GDGT-1 +
256 GDGT-2 + GDGT-3 + cren')

257

258 This proxy is based on the physiological relationship in which the degree of cyclisation in
259 GDGTs is correlated to temperature (De Rosa et al., 1980; Gliozzi et al., 1983; Uda et al.,
260 2001). $Ring_{AV}$ is a normalised form of the Ring Index proposed by Zhang *et al* (2016) as a
261 guide to situations where TEX_{86} has been influenced by non-thermal factors or deviates from
262 modern analogue relationships. Other potential sources of bias related to physiology,
263 seasonality and water depth have been widely discussed (e.g., Turich et al*.,* 2007; Kim et al*.,*
264 2008; Huber and Caballero, 2011; Hollis et al., 2012; Taylor et al., 2013; Hernandez-
265 Sanchez et al., 2014; Ho and Laepple, 2016). TEX_{86} values can also be biased by the input
266 of terrestrial GDGTs but this bias is considered to be negligible when the branched vs.
267 isoprenoid (BIT) index is lower than 0.3 (Weijers et al., 2006). The BIT index is also a useful
268 proxy from terrestrial input.

BIT = (bGDGT-I + bGDGT-II + bGDGT-III) / (bGDGT-I + bGDGT-II + bGDGT-III + crenarchaeol),

where I, II and III refer to brGDGTs with no rings and 4, 5 or 6 methyl groups, respectively (Schouten et al., 2012).

3. Results and Discussion

In this section, we outline the biostratigraphic basis for age control in the mid-Waipara section. We describe the trends in GDGT and interpret the trends in relation to SST reconstructions and changes in dinoflagellate assemblages. We compare the mid-Waipara section to the more complete Branch and Mead stream sections in Marlborough. We conclude the section by discussing the nature and possible causes on long-term trends climatic and environmental conditions the followed the K/Pg boundary event.

3.1. Biostratigraphy of the mid-Waipara section

The primary age control for the mid-Waipara section is provided by dinoflagellates (Willumsen,2003; 2004; 2006; 2012). Age control for dinoflagellate events is based primarily on correlation with foraminiferal and radiolarian biostratigraphy in the Branch and Mead stream sections in southeastern Marlborough (Hollis et al., 2003a; Willumsen, 2003; 2011; 2012; Crouch et al., 2014). The co-occurrence of all three fossil groups in these sections has been utilised to develop a well-resolved event stratigraphy (Supplementary materials S5).

Despite the evidence for bioturbation across the K/Pg boundary at mid-Waipara, several lines of evidence suggest that the boundary is intact and earliest Paleocene sediments are preserved. Geochemical studies indicate that the boundary is enriched in Ir and other siderophiles (Fig. 2; Brooks et al., 1986; Hollis and Strong, 2003; Ferrow et al., 2011).

Foraminiferal assemblages also indicate that the lowermost Paleocene sample can be correlated to earliest Paleocene zone P0 and the overlying sample can be correlated with zone Pα (Hollis and Strong, 2003). Dinoflagellate biostratigraphy indicates that the basal Paleocene (0-22 cm above the K/Pg boundary) can be correlated with lower NZDP1, based on the co-occurrence of *Trithyrodinium evittii, Senoniosphaera inornata,* and *Manumiella druggii.* The first two species have lowest occurrences (LOs) at the K/Pg boundary in New Zealand whereas the highest occurrence (HO) of *M. druggii* occurs within the lower part of zone NZDP1, coincident with the base of radiolarian zone RP2 in the Branch and Mead Stream sections. At mid-Waipara, bioturbation is inferred to have resulted in the occurrence of *T. evittii* in the uppermost Cretaceous, an inference supported by Ferrow et al. (2011). Ferrow et al. (2011) also reported the LOs of *Damassadinium californicum* and *Membranilarnica*? *tenella* directly above the K/Pg boundary. The LO of *D. californicum* is a global marker for the earliest Paleocene. The LO of *M.*? *tenella* was initially thought to occur later, close to the top of foraminiferal zone P0 according to Brinkhuis and Zachariasse (1988; see also Habib et al., 1996). However, more recent studies have established that the species is present in small numbers from the base of the Paleocene (Vellekoop et al., 2015). Furthermore, several latest Maastrichtian to earliest Paleocene species (*Carpatella septatum, C. truncata, Impagidnium cavea, I. agremon, Pyxidiniopisis epakros and P. everriculum*) have their HO between 0.16 and 0.325 above the K/Pg boundary.

Crouch et al. (2014) provide an age estimate of ~65.4 Ma (earliest zone RP2) for the HO of *Manumiella druggii*. In this section, we place this event at the rapid decrease in the abundance of *M. druggii* between 0.20 and 0.225m. We interpret rare occurrences and isolated occurrence above this level as being due to reworking. This interpretation is consistent with the HO of *Trichodinium hirsutum* at 0.475 m. This event occurs above the HO of *M. druggii* in the Mead and Branch sections and is dated at ~65.1 Ma by Crouch et al. (2014). Consequently, the interval from 0.475 to 0.725 m is correlated with uppermost zone NZDP1 based on the absence of *M. druggii* and HO *T. hirsutum* in the basal sample. The

interval from 0.725 m to the top of the studied section is correlated with zone NZDP2 based on the co-occurrence of *Cerodinium striatum* and *Trithyrodinium evittii*.

An age depth plot for the section (Supplementary materials S6, S7) indicates that there is a significant unconformity at the level of the second Fe-stained layer (0.23 m). A sample directly above the unconformity (M34/f124; Hollis and Strong, 2003) contains the LO of foraminifer *Parvulorugoglobigerina eugubina*, which marks the base of foraminiferal zone Pα (66 Ma). This implies that the interval below the unconformity lies within zone P0 and represents no more than 40 kyrs. Because two dinoflagellate events occur at the same stratigraphic level as this foraminiferal event but have significantly younger ages (HO *M. druggii*, ~65.4 Ma; HO *T. hirsutum* ~65.1 Ma), this unconformity is inferred to represent a hiatus of ~1 Myr (Fig. 2). As noted above, the HOs of several other dinoflagellate species have been noted at the level of this unconformity. The unconformity also marks the top of the K/Pg fern spike (Vajda et al., 2001; Vajda and Raine, 2003; Ferrow et al., 2011), with the abundance of fern spores decreasing from 66 to 22% of the total miospore assemblage. There are no indications of other significant unconformities in the section, with a modest sedimentation rate of 5.75 m/Ma estimated for the K/Pg boundary transition and a higher rate of 14.63 m/Ma determined for the interval above the unconformity.

3.2. Organic Geochemistry

Total organic carbon (TOC; Fig. 4A) is generally low (< 0.5 wt %) through the K/Pg transition and falls to a minimum between 0.22 and 2 m above the boundary (<0.3 wt %). Biomarker distributions across throughout the section indicate both terrestrial and marine sources for organic matter (OM), with high-molecular-weight (C_{27}-C_{31}; HMW) *n*-alkanes with a relatively strong odd-over-even predominance and HMW (C_{28}-C_{32}) *n*-alkanoic acids with a strong even-over-odd predominance indicating a significant terrigenous contribution (Supplementary materials S4; Eglinton and Hamilton, 1963, 1967; Cranwell *et al.,* 1987).

The presence of branched GDGTs (bGDGTs) indicates fluvially transported soil organic matter input (Fig. 3; Hopmans et al., 2004; Weijers et al., 2006). However, BIT indices are relatively low (< 0.11; see Supplementary materials S8) throughout, indicating a relatively small terrestrial component of OM relative to marine (Hopmans et al., 2004, Weijers et al., 2006). Marine contributions are evident not only from the low BIT indices but also abundant low molecular weight (C_{14} – C_{20}; LMW) *n*-alkanoic acids with an even-over-odd predominance (Supplementary materials S4; e.g. Volkman et al., 1980; Claustre et al., 1989; Carrie et al., 1998) and relatively high concentrations of pristane and phytane (e.g. Dean and Whitehead, 1961; Rontani and Volkman, 2003).

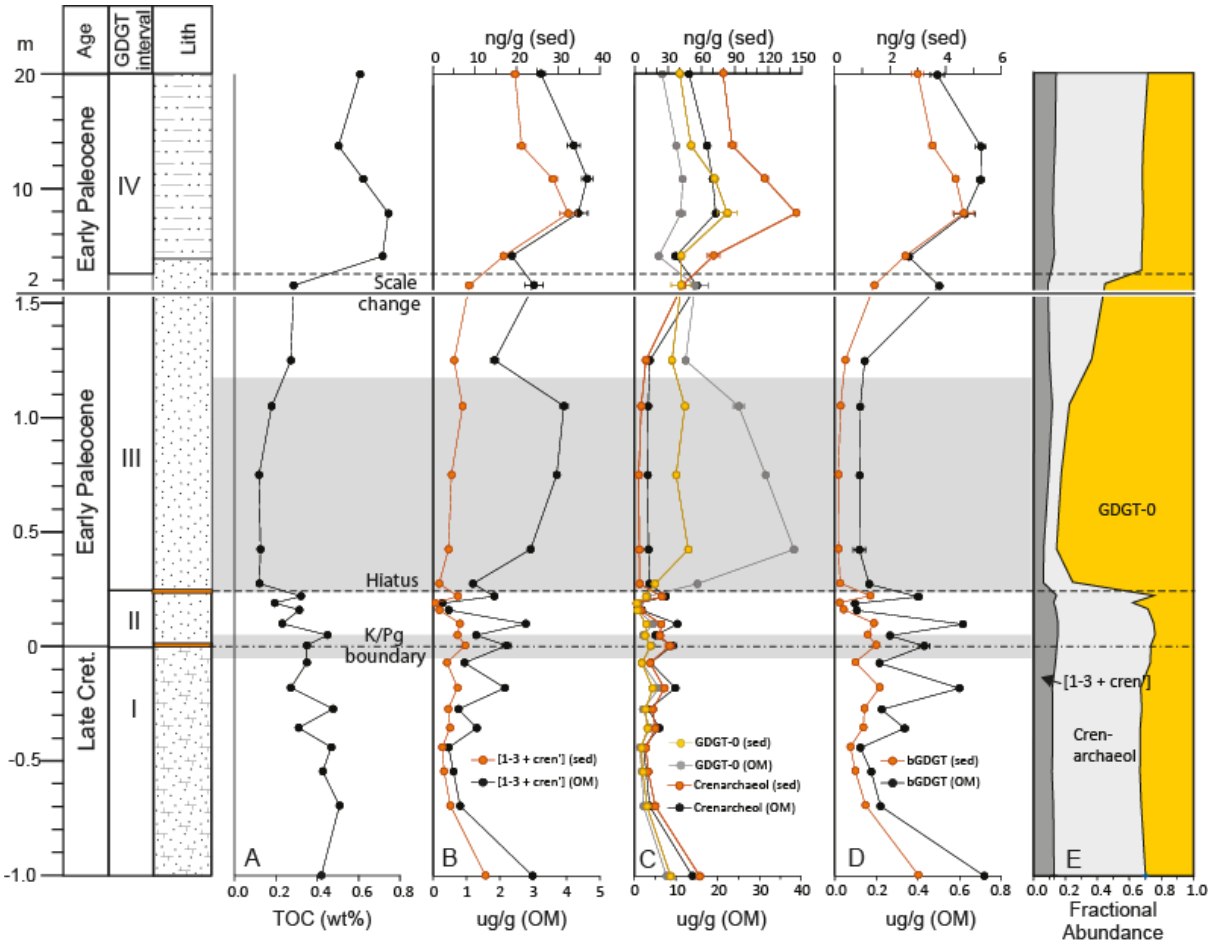

Figure 3. Organic geochemical profiles through the K/Pg transition at mid-Waipara River: (A) total organic carbon (TOC); semi-quantitative concentrations of GDGTs in bulk sediment and

organic matter, including (B) [1-3 & cren'], (C) crenarchaeol and GDGT-0, and (D) branched GDGTs; (E) fractional abundance of GDGT-0, crenarchaeol and [1-3 + cren']. Note the scale change above 1.5 m sample depth.

3.3 GDGT concentrations and distributions

We previously reported the distributions of GDGTs in the Paleocene at mid-Waipara River in terms of $Ring_{av}$ and tetraether indices (TEX_{86}^{H} and TEX_{86}^{L} and their respective SSTs), as well as the offset between those two SST proxies (Δ H-L) as a function of [2]/[3] ratios (Taylor et al., 2013). Here, we expand those analyses and further interrogate variation in GDGT distributions and concentrations across the K/Pg boundary. In addition to these two SST proxies, we consider TEX_{86}[linear], $pTEX_{86}$, $BAYSPAR_{SST}$, $BAYSPAR_{SubT}$ and SPM-TEX_{86}.

Branched and isoprenoidal GDGT concentrations exhibit similar trends to those described for TOC (Fig. 3B-D). Isoprenoidal GDGT concentrations are generally an order of magnitude higher than those of branched GDGTs and crenarchaeol is the dominant GDGT (Fig. 4E). Concentrations of all GDGTs are low in the uppermost Cretaceous and exhibit fluctuations across the K/Pg boundary. Summed GDGTs 1, 2, 3, and cren' (herein denoted as [1-3 + cren']) concentrations (Fig. 4B), GDGT-0 and crenarchaeol (Fig. 3C) have small peaks at or directly above the K/Pg boundary. Above the unconformity at 0.23 m, there is a sharp increase in the concentration of GDGT-0 (Fig. 3C), concomitant with a decrease in concentrations of all other isoprenoidal and branched GDGTs (Fig. 3B-E). Concentrations of GDGT-0 remain high and dominate the GDGT distribution from 23 cm to 1.15 m (Fig. 3E). Concentrations of crenarchaeol and brGDGTs increase from ~2 m above the K/Pg boundary as GDGT-0 decreases (Fig. 3C-E) and the proportions of GDGT-[1-3 + cren'], GDGT-0 and crenarcheol return to values similar to those recorded in the uppermost Cretaceous (Fig. 3E). Maximum concentrations of all GDGTs other than GDGT-0 occur in the lower Loburn

Formation (4−12 m), before gradually decreasing in the upper part of the section. These trends persist even when concentrations are normalised to TOC content (Fig. 3B-D; also see Supplementary materials S4).

Based on these trends, as well as distributions of the TEX86-related GDGTs, four distinct intervals are evident in the K/Pg section (Fig. 4, 5, 6A):

(I) Upper Cretaceous (-1.2 to -0.18 m): moderate TOC, low GDGT concentrations, dominated by crenarchaeol.

(II) Uppermost Cretaceous and basal Paleocene (-0.07 to 0.22 m): fluctuating TOC and GDGT concentrations, also dominated by crenarchaeol but with higher abundance of GDGT-2.

(III) Lower Paleocene (0.22 to ~2 m): minimum TOC contents and GDGT concentrations, but high fractional abundance of GDGT-0, GDGT-1 and GDGT-2

(IV) Lower Paleocene (~2 to 20 m): maximum TOC contents and GDGT concentrations, dominated by crenarchaeol.

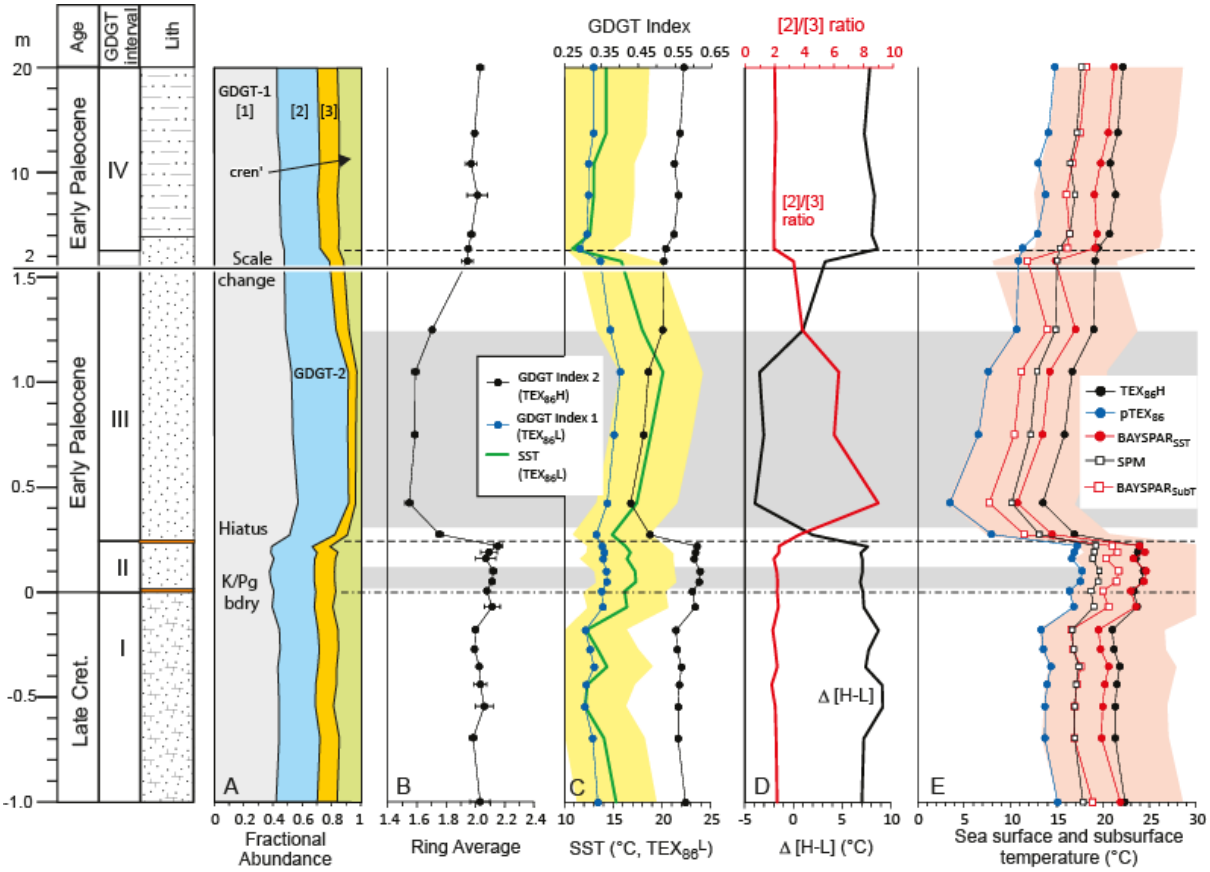

Figure 4. GDGT-based indicators of sea temperature change through the K/Pg transition at mid-Waipara River: (A) fractional abundance for GDGT-1 , -2, -3 and cren'; (B) $Ring_{AV}$; (C) TEX86 and TEX86L indices, with TEX_{86}^{H} and TEX_{86}^{L}-reconstructed SSTs (calibration error of +/-4°C is shaded); (D) SST offset between TEX_{86}^{L} and TEX_{86}^{H} calibrations (ΔH-L) and [2]/[3] ratio, highlighting unusual behaviour in Interval III; (E) Sea surface and subsurface temperature profiles based on TEX_{86}^{H}, $pTEX_{86}$, $BAYSPAR_{SST}$, $BAYSPAR_{subT}$ and SPM-TEX_{86}, the pink shaded interval is the 95th confidence interval based on BAYSPAR. Note the scale change above 1.5 m sample depth.

3.4 Sea surface temperature reconstructions

The fractional abundance of the GDGTs that are used for temperature reconstructions are relatively consistent for Intervals I, II and IV. However, the abundance of GDGT-1 and

GDGT-2 are significantly elevated relative to GDGT-3 and cren' in Interval III (Fig. 4A). As previously noted, the proportion of GDGT-0 is also markedly higher in Interval III. These relationships are captured in $Ring_{AV}$ (Fig. 4B), which increases slightly from Interval I to Interval II but then decreases markedly across the unconformity at 23 cm from Interval II to Interval III. The parameter increases in the upper part of Interval III and then is stable through Interval IV with values similar to Interval I.

Trends in TEX_{86} typically parallel trends in $Ring_{AV}$ because both indices are based on the number of cyclopentane moieties. In the mid-Waipawa section, TEX_{86} also has a maximum within Interval II and a minimum within Interval III (Fig. 4C), which is interpreted to indicate an interval of warmer conditions directly above the K/Pg boundary (Interval II) followed by cooling in Interval III (Fig. 4D). However, the same correlation is not observed between $Ring_{AV}$ and TEX_{86}^{L}. Relationships between the two indices are consistent for Intervals I, II and IV but for Interval III, TEX_{86}^{L} increases, which implies higher rather than lower SSTs (Fig. 4C). This anomaly is explained by the unusually high abundance of GDGT-2 relative to GDGT-3 in this interval. Because GDGT-2 is the sole numerator in the TEX_{86}^{L} equation, any increase in its concentration will shift the proxy to warmer temperatures.

Taylor et al. (2013) showed that these unusual variations in the relative abundance of GDGT-2 and GDGT-3 (expressed as the [2]/[3] ratio) can invert the normal relationship between the TEX_{86}^{L} and TEX_{86}^{H} proxies in which the latter tends to yield warmer SSTs than the former (i.e. positive ΔH-L). Interval III at mid-Waipara is a striking example of this situation, in which an increase in the [2]/[3] ratio results in the negative ΔH-L (Fig. 4D). Taylor et al. (2013) found that the [2]/[3] ratio appeared to increase with water depth both in sediments and suspended particulate matter (in both core and intact lipids with respect to the latter), a finding that has since been corroborated in other studies (e.g. Hernandez-Sanchez, 2014; Kim et al., 2015), including within intact polar lipids (Lengger et al., 2012;

445 Schouten et al., 2012). The shift in ratio has been ascribed to changes in subsurface
446 thaumarchaeal ecology (Villaneuva et al., 2015) and may indicate a greater proportion of
447 GDGT export from subsurface waters (e.g. Taylor et al., 2013; Hernandez-Sanchez, 2014;
448 Ho and Laepple, 2016).
449
450 Further evidence for unusual environmental or ecological conditions in Interval III comes
451 from the increase in concentration of GDGT-0 and the marked decrease in other GDGT
452 concentrations (Fig. 3B-E). GDGT-0 is not used in GDGT temperature calculations because
453 it can be derived from multiple sources, including not only Thaumarchaeota but also
454 sedimentary Archaea (Schouten et al., 2002). In modern and Paleogene sediments it is very
455 uncommon to find GDGT-0 relative abundances as high as those observed in Interval III
456 (Inglis et al., 2015). It is most abundant in cool polar settings (although rarely >60% of the
457 GDGT assemblage; Schouten et al., 2002) and in anoxic lacustrine settings (Blaga et al.,
458 2009). Although low TOC and extensive bioturbation suggest relatively oxic sea-floor
459 conditions during Interval III, the enrichment in Cr noted above (Fig. 2) is consistent with
460 some degree of dysoxia (Calvert and Pedersen, 1993).
461
462 In summary, a greater proportion of export from the subsurface relative to surface waters
463 could account for the high abundance of GDGT-2 and the unusual temperature trend derived
464 from TEX_{86}^{L} within Interval III. Moreover, the high abundance of GDGT-2 and GDGT-0 in this
465 interval suggests an environment in which sub-surface or sedimentary Archaea are major
466 contributors to the GDGT assemblage (Fig. 3E, 4A) and in which there is an overall
467 decrease in the export of GDGTs from the surface waters (i.e. GDGT-3, cren' and
468 crenarchaeol).
469
470 These factors have little impact on TEX_{86}^{H} because GDGT-2, GDGT-3 and cren' are
471 incorporated into both the numerator and denominator in the equation. As all other GDGT-
472 based temperature calibrations are based on this index, they are considered to reliably

record the general temperature trend through the mid-Waipara K/Pg section (Fig. 4E). To examine this in more detail, we have calculated temperatures using six calibrations based on TEX_{86}^{H}. For SSTs, we have used TEX_{86}^{H}, TEX_{86}[linear], $pTEX_{86}$ and $BAYSPAR_{SST}$. We have also calculated subsurface temperatures using $BAYSPAR_{SubT}$ and SPM-TEX_{86}. As expected, all calibrations yield very similar trends but differ considerably in absolute values, although all values lie within the uncertainty bounds of $BAYSPAR_{SST}$. Absolute SSTs are similar for TEX_{86}^{H} and $BAYSPAR_{SST}$ whereas $pTEX_{86}$ yields SSTs that are ~7°C cooler and align closely with the lower limit for $BAYSPAR_{SST}$. SPM-TEX_{86} and $BAYSPAR_{SubT}$ are in close agreement and yield values that are intermediate between $pTEX_{86}$ and TEX_{86}^{H}.

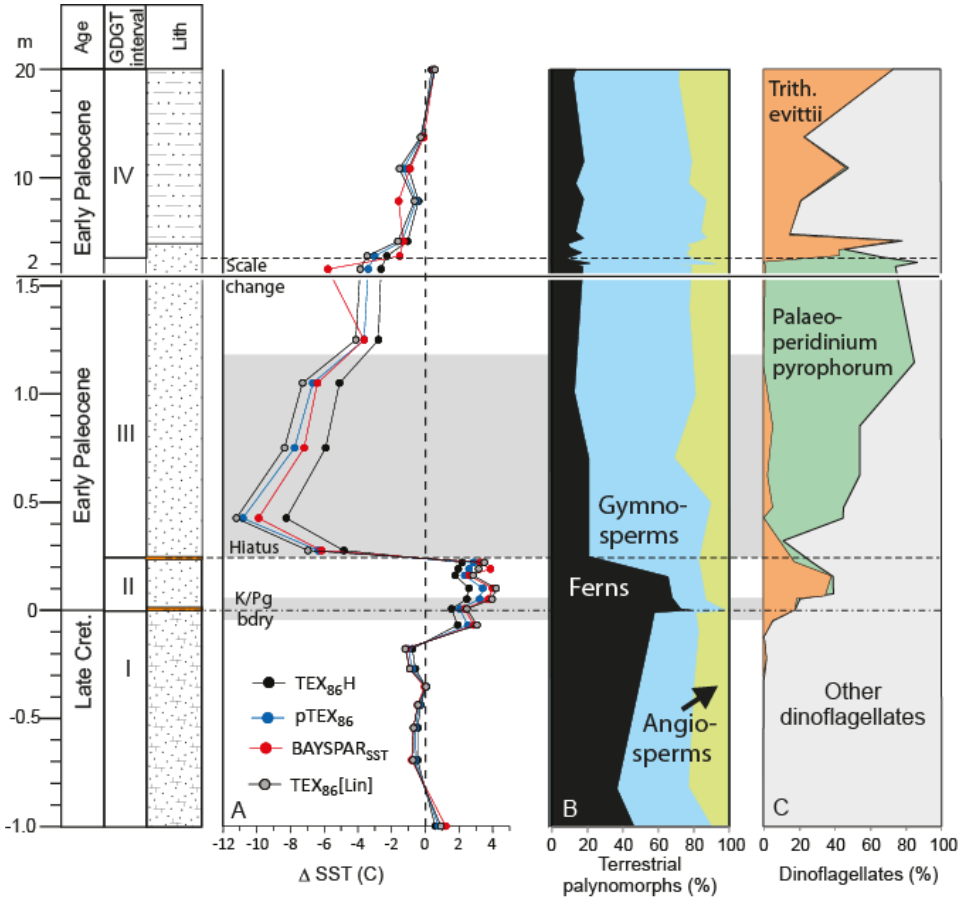

Figure 5. Comparison of the relative SST profile with the floral and microfloral turnover events through the KPB transition at mid-Waipara River: (A) Variation in SST relative to mean SST for Interval I (Cretaceous) for TEX_{86}^{H}, $pTEX_{86}$, $BAYSPAR_{SST}$, and TEX_{86}[linear]; (B) relative abundance of ferns, gymnosperms and angiosperms (from Vajda and Raine,

2003); (C) relative abundance of two dinoflagellate species Trithyrodinium evittii and Palaeoperidinium pyrophorum. Note the scale change above 1.5 m sample depth.

Because of this wide variation in absolute temperatures, we outline the primary features of the record in terms of variation in temperature from average Cretaceous values (Δ SST) (Fig. 5A). A weak cooling trend of ~2°C is evident in the upper Cretaceous (Interval I). This trend is reversed in the uppermost Cretaceous where temperatures warm abruptly by ~3-4°C. SST is variable within Interval II, ranging from 2 to 4°C warmer than average Cretaceous values and with an SST peak directly above the K/Pg boundary. The warming in the uppermost Cretaceous could be interpreted as warming preceding the K/Pg event, but dinoflagellates and inorganic geochemistry indicate that basal Paleocene sediments have been worked down into the uppermost few centimetres of Cretaceous strata by bioturbation.

SSTs within Interval III exhibit a clear trend: pronounced cooling at the base is followed by progressive warming. Depending on the calibration, the initial decrease in temperature is between 7 and 11°C and the overall decrease from the maximum in Interval II to the minimum in Interval III is between 10 and 15°C. Minimum SSTs in Interval III are 8-11°C cooler than the average for the Cretaceous. This is very clear evidence for an episode of pronounced cooling at the base of Interval III. SST warms in the upper part of Interval III and into Interval IV, returning to Cretaceous levels ~15 m above the K/Pg boundary.

3.5. Palynological indications of environmental change

A dramatic turnover in vegetation is recorded in the pollen and spore assemblages that span the K/Pg boundary transition at mid-Waipara River (Vajda et al., 2001; Vajda and Raine 2003; Ferrow et al., 2011). A mixed forest assemblage in the uppermost Cretaceous is replaced by an assemblage dominated by fern spores in the basal Paleocene (Fig. 5B). Ferns dominate assemblages up to the unconformity at 0.22 m above the boundary.

Assemblages are dominated by gymnosperms above the unconformity and to the top of the examined section (30 m above the K/Pg boundary). An equivalent record of floral turnover is found in a non-marine K/Pg boundary record on the west coast of the South Island (Vajda et al., 2001). In both sections, the fern spike comprises a floral succession with ground ferns at the base giving way to tree ferns. Vajda et al. (2001) interpreted this succession as signifying (i) devastation of forests at the K/Pg boundary, (ii) colonisation of open areas by ground ferns, (iii) expansion of tree ferns under warm temperate conditions, and (iv) expansion of gymnosperms under cooler conditions, as evident from the abundance of *Phyllocladidites mawsonii*, a pollen species thought to be closely related to the cool-temperate rain forest conifer *Lagarostrobos franklinii (*Huon Pine).Our temperature record supports this interpretation. The fern spike is correlated with Interval II and the lower part of the conifer interval corresponds with Interval III. However, given that conifers continue to dominate Interval IV, other factors appear to be implicated in the delayed recovery of a mixed angiosperm-gymnosperm forest.

In addition to the terrestrial palynomorph record, the mid-Waipara section is rich in marine palynomorphs, primarily dinoflagellate cysts. The dinoflagellate record provides a valuable means to correlate with other K/Pg boundary sections in New Zealand and also provides further insights into environmental changes during this time period. The K/Pg transition is distinguished by a succession of assemblages, including the alternating abundance of two dominant species, *Trithyridinium evittii* and *Palaeoperidinium pyrophorum* (Fig. 5C). Both species are inferred to be heterotrophic peridinioids, which have been associated with various types of nutrient-rich settings and salinities (Dale, 1996; Askin, 1988; Habib et al., 1994; Evitt et al., 1998; Sluijs et al., 2005).

Interval II corresponds with an acme in *Trithyrodinium evittii*, which is inferred to be a warm-water species (Brinkhuis et al., 1998; Nøhr-Hansen and Dam, 1997; 1999; Willumsen, 2003; Willumsen and Vajda, 2010b; Vellekoop et al., 2015). As noted above, the initial increase in

T. evittii is observed directly below the K/Pg boundary where the species makes up > 6% of the assemblage. It increases to 18% of the assemblage directly above the boundary. Interval III corresponds with an acme in *Palaeoperidinium pyrophorum*, a species that is abundant in lowermost Paleocene marginal marine sediments on Seymour Island (Askin, 1988) and the southwest Tasman Sea (Brinkhuis et al., 2003) as well as the pelagic bathyal sequence in eastern Marlborough (Willumsen, 2003; 2006; 2011; Willumsen and Vajda, 2010a; 2010b). These two acmes appear to agree well with the TEX_{86} record, with abundant *T. evittii* in the warm basal Paleocene interval and the high-latitude species, *P. pyrophorum*, dominating in the overlying cool interval.

4. Correlation and comparison with other New Zealand records

4.1. Biostratigraphic correlation

The TEX_{86} warming event (Interval II) occurs within foraminiferal zone P0 and the TEX_{86} cooling event (Interval III) occurs within upper dinoflagellate zone NZDP1 to lower NZDP2 (Fig 6). Additional dinoflagellate and radiolarian bioevents allow us to correlate these intervals with coeval sedimentary successions in the Mead and Branch Stream K/Pg boundary sections (Fig. 6). As noted above, these two climate events are correlated with distinct dinoflagellate acmes: the *T. evittii* acme (Te1) and the overlying *P. pyrophorum* acme (Pp1). At mid-Waipara, Te1 is very condensed and the Te1/Pp1 transition is only 23 cm above the boundary, coinciding with the unconformity. However in the Mead and Branch sections the Te1/Pp1 transition is 2.35 and ~12 m above the K/Pg boundary, respectively. Correlation lines based on the primary dinoflagellate and radiolarian bioevents in the three sections show that the two dinoflagellate acme intervals, Te1 and Pp1, are separated by ~1 Myr. Interval II is correlated with foraminiferal zone P0, which encompasses the first 40 kyrs of the Paleocene. We cannot determine if Interval II spans this entire time period or represents a short-lived event within it. Interval III is dated at ~65 Ma based on two well-

defined datums, the base of *Cerodinium striatum* near the base of Pp1 and the base of *Buryella granulata* in the upper part (Fig. 6). It is possible that the unconformity at mid-Waipara corresponds with the Da2 sequence boundary of Hardenbol et al. (1998).

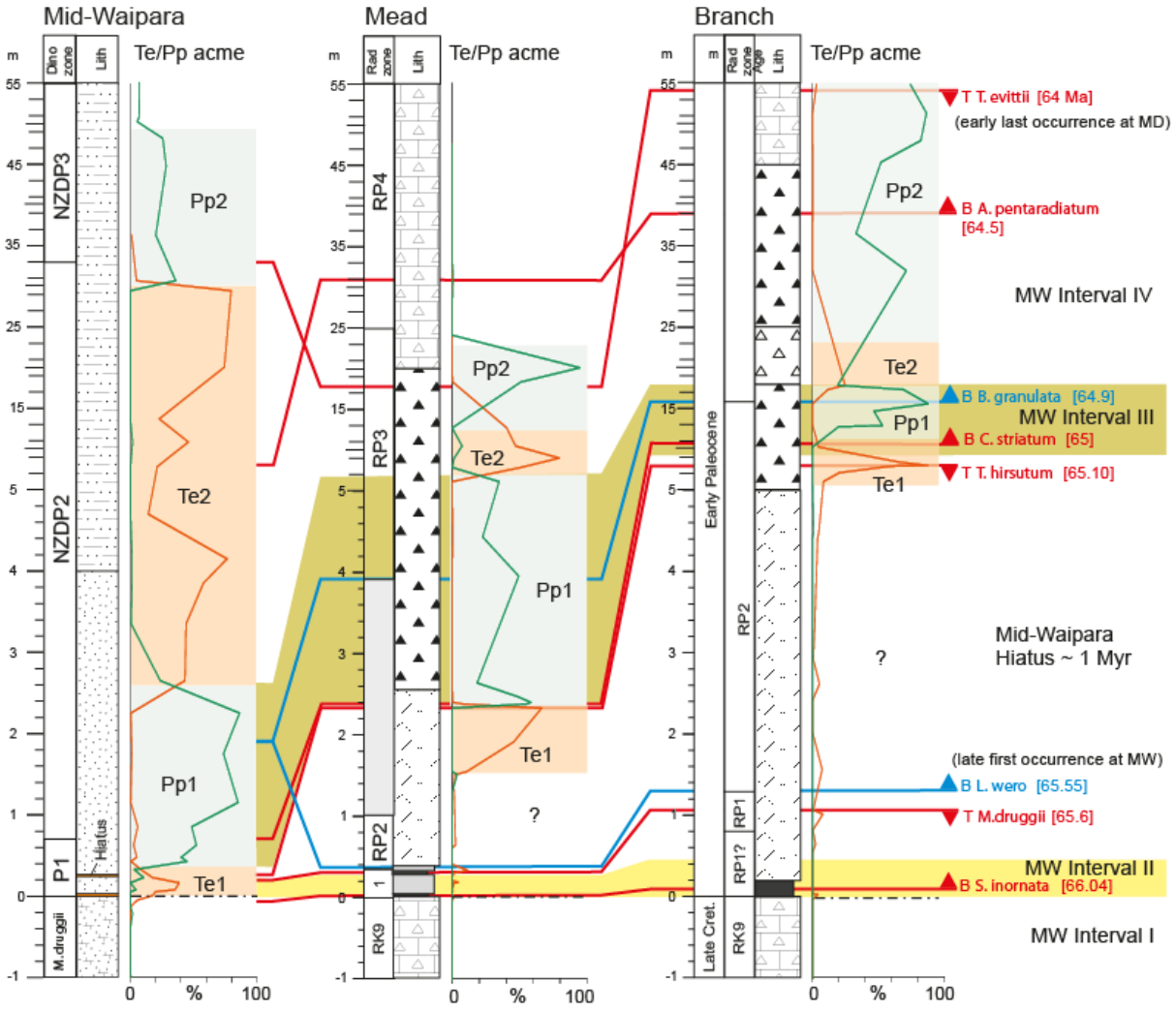

Figure 6. Correlation of GDGT Intervals I to IV in the mid-Waipara section to the Mead and Branch Stream sections based on bioevents and acmes in the dinoflagellate species Trithyrodinium evittii (Te1 and TE2) and Palaeoperidinium pyrophorum (Pp1 and Pp2). Lithology and selected index taxon FODs and LODs are indicated on the figure. Blue = radiolarian; Red = dinoflagellates. Note the scale change above 1.5 m sample depth.

Correlation also shows that the Te1 acme is diachronous, occurring in the earliest Paleocene at mid-Waipara, but almost 1 Myr later at Mead and Branch Stream. We suspect that this diachroneity reflects the deeper water and possibly cooler oceanic setting of the Marlborough sections. The implication that other dinoflagellate taxa occupied the warm-water niche in these deep-water sites prior to the expansion of *T. evittii* is explored below.

4.2 Paleoenvironmental significance of dinoflagellate cyst acmes

Variations in the abundance of some dinoflagellate cyst taxa can be used to refine interpretation of environmental changes in these sections. In particular, changes in assemblages through the expanded Branch section provide context for the truncated climate record at mid-Waipara. We have reviewed what is known of the environmental preferences of eight dinoflagellate taxa and apply this information to the three sections (Fig. 7-9).

Trithyrodinium evittii is considered to be a warm-water indicator, being common in low latitudes in the latest Cretaceous and migrating to high latitudes during an interval of global warming in the earliest Paleocene (Nøhr-Hansen and Dam, 1997, 1999; Brinkhuis et al., 1998; Willumsen, 2003; Vellekoop et al., 2015). This is consistent with the first *T. evittii* acme at mid-Waipara (Te1) occurring within Interval II and the second (Te2) being associated with warm SSTs within Interval IV. The large spikes in *T. evittii* abundance in Branch and Mead Stream sections that occur directly below the Pp1 acme may reflect post-depositional transport of an earlier Paleocene assemblage dominated by *T. evittii*, perhaps as part of the shelfal erosional event that caused the unconformity at mid-Waipara.

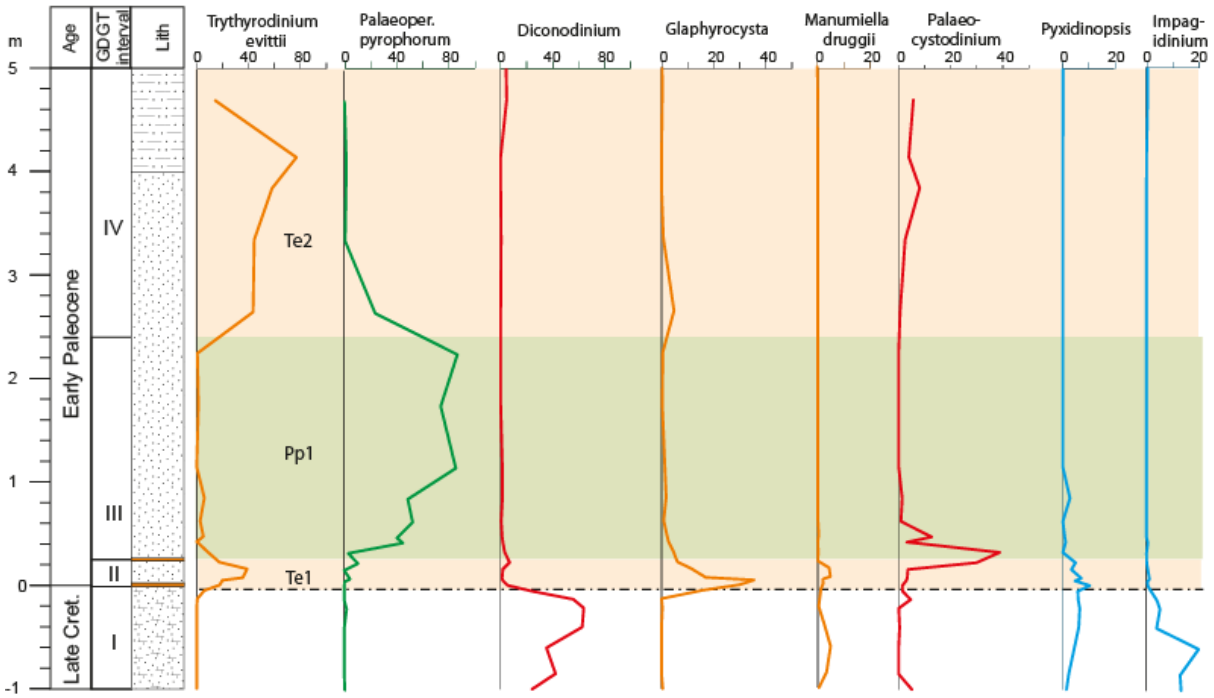

598

599 *Figure 7. Relative abundance of selected dinoflagellate taxa in the uppermost Cretaceous*
600 *and lower Paleocene at mid-Waipara River, north Canterbury. The intervals correlated with*
601 *the Trithyrodinium evittii (Te1 and TE2) and Palaeoperidinium pyrophorum (Pp1) acmes are*
602 *shaded.*

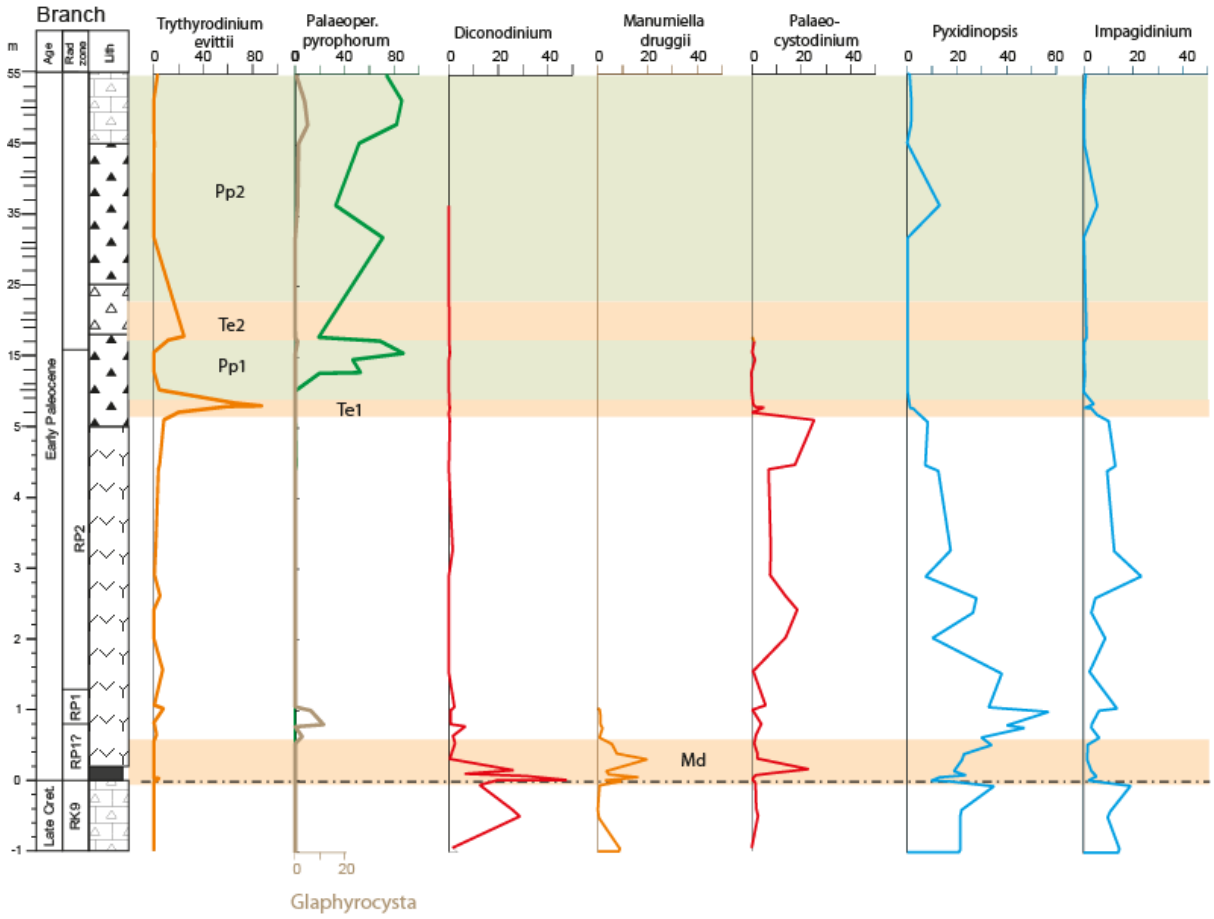

603

604 *Figure 8. Relative abundance of selected dinoflagellate taxa in the uppermost Cretaceous*
605 *and lower Paleocene at Branch Stream, eastern Marlborough. The intervals correlated with*
606 *the Trithyrodinium evittii (Te1 and Te2) and Palaeoperidinium pyrophorum (Pp1 and Pp2)*
607 *acmes and a basal Paleocene interval with abundant Manumiella druggii (Md) are shaded.*
608 *Note the scale change above 1.5 m sample depth.*

609

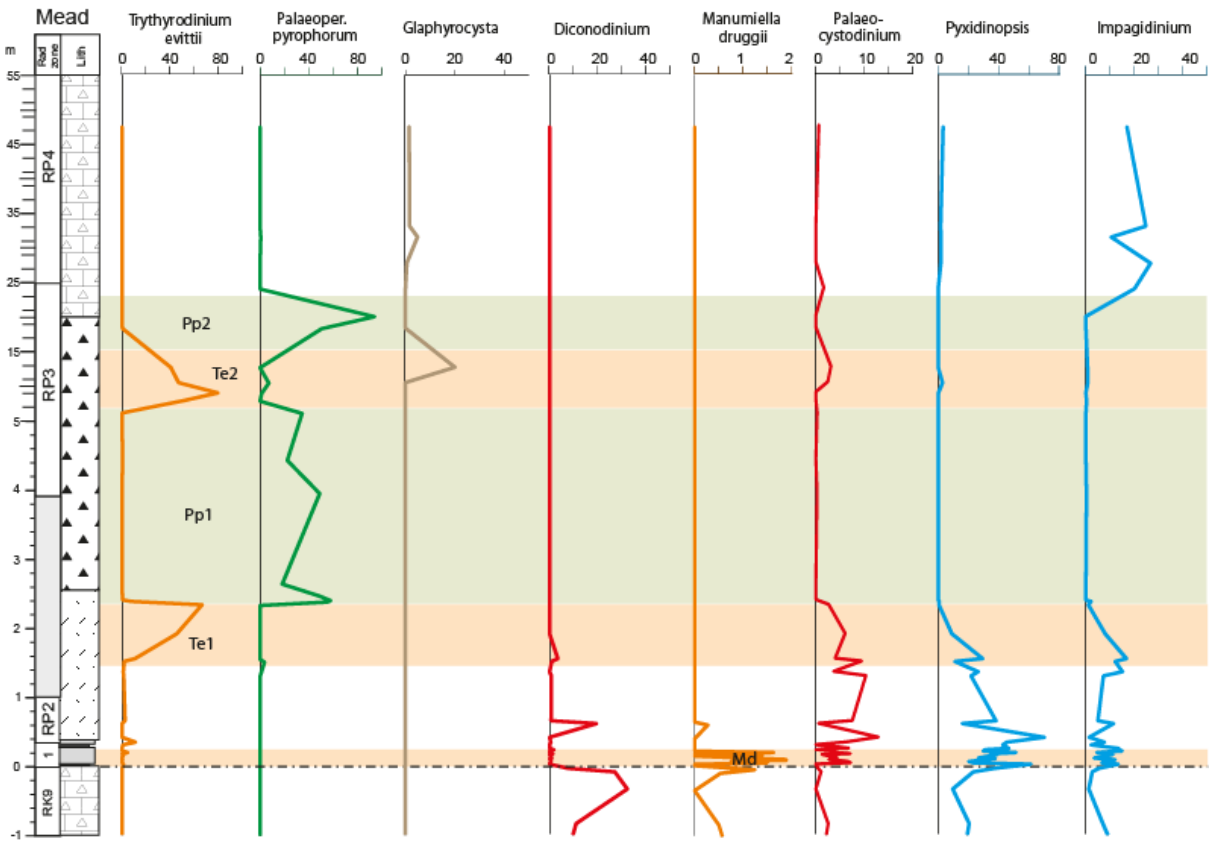

Figure 9. Relative abundance of selected dinoflagellate taxa in the uppermost Cretaceous and lower Paleocene at Mead Stream, eastern Marlborough. The intervals correlated with the Trithyrodinium evittii (Te1 and Te2) and Palaeoperidinium pyrophorum (Pp1 and Pp2) acmes and a basal Paleocene interval with abundant Manumiella druggii (Md) are shaded. Note the scale change above 1.5 m sample depth.

Abundant ***Palaeoperidinium pyrophorum*** has been interpreted to represent a wide range of environments from fully marine to restricted marine stressed conditions with low salinity and extreme pH-values (Evitt et al., 1998; Askin, 1988; Habib et al., 1994). Acmes have been reported in a neritic setting of Seymour Island (Askin, 1988) as well as in pelagic sediments from the Viborg-1 corehole, onshore Denmark (Heilmann-Clausen, 1985). We also find that both *P. pyrophorum* acmes (Pp1 and Pp2) occur in three sections representing

a transect from shelf to upper slope (Fig. 8B). Both the Danish and New Zealand studies report high absolute abundance of cysts in the Pp acme intervals with up to 770,000 specimens per gram of sediment (Heilmann-Clausen, 1985; Willumsen, 2006; 2011). It appears that Pp acme intervals are either restricted to high latitudes or associated with siliceous microfossils, as is seen in Seymour Island (Askin, 1988; Harwood, 1988), California (Drugg, 1967; Foreman, 1968) and New Zealand. The Pp1 and Pp2 acmes span the main interval of siliceous microfossil-rich sediments in the early Paleocene of the Mead Hill Formation in Marlborough (upper radiolarian zone RP2 to upper RP3, 65-64 Ma) (Willumsen, 2006; 2011) (Fig. 6). We infer that the Pp acmes in the New Zealand sections reflect cooling or coastal upwelling of cool, nutrient rich waters, consistent with the correlation between Pp1 and TEX_{86} cooling in Interval III.

Manumiella druggii has been interpreted as representing restricted shallow marine conditions (Hultberg, 1987; Firth, 1987; Askin and Jacobsen, 1996). Brinkhuis et al. (1998) interpreted increases in abundance in the earliest Paleocene in high latitudes to be an indication of warming. However, Habib and Saeedi (2007) found a spike in abundance coincident with latest Cretaceous cooling inferred from planktic $\delta^{18}O$ in the Brazos River K/Pg section. This appears to be supported by subsequent assemblage analysis by Vellekoop et al. (2015). However, both these records are from low latitude sites. We observe a small increase in abundance in the basal Paleocene within the Te1 acme at mid-Waipara (Fig. 7), and a slightly larger increase in abundance at Branch Stream in the interval correlated with the warming event (Fig. 8). The species is very rare at Mead Stream, but has a brief acme (~2%) directly above the K/Pg (Fig. 9). In line with the interpretation of Brinkhuis et al. (1998), we interpret this pattern of *Manumiella* occurrence to indicate that *M. druggii* is a temperate-water species that increases in abundance in high-latitudes during times of relative warmth but in low latitudes may increase during times of relative cooling.

Diconodinium and ***Palaeocystodinium*** are considered to be warm-water indicators (Fensome et al., 1993; Brinkhuis et al., 1998; Vellekoop et al., 2015). However, neither

genus is common during GDGT Interval II at mid-Waipara. *Diconodinium martianium* is common in the uppermost Cretaceous in all sites but becomes very rare in the Paleocene at mid-Waipara and Mead (Fig. 7, 9) and represents a latest Maastrichtian marine floral element. At Branch Stream, however, a significant peak in abundance occurs directly above the K/Pg boundary. *Palaeocystodinium* is rare in the uppermost Cretaceous, exhibits a small increase in the basal Paleocene and is common to abundant in the interval between Intervals II and III (Fig. 8). As such, these taxa are interpreted as warm-water indicators, but perhaps not as warm as indicated by *T. evittii*.

The gonyaulacoid genera ***Impagidinium*** and ***Pyxidinopsis*** are considered to be more common in more oceanic settings (Dale, 1996; Willumsen, 2003; Crouch and Brinkhuis, 2005; Vellekoop et al., 2015) and as such are proxies for oceanicity or proximity to shoreline. This agrees with the observations made here, with both taxa more common at the pelagic Branch and Mead sections compared with assemblages from the siliciclastic mid-Waipara River section. Significantly, the abundance of *Impagidinium* decreases across the K/Pg boundary at mid-Waipara and Branch (Willumsen 2003; 2011). This could reflect a fall in sea level because this decrease is not observed at the Mead section, which represents the deepest depositional setting (Hollis et al., 2003a).

Pyxidinopsis exhibits an interesting pattern in the expanded Branch section: decreasing across the K/Pg boundary, followed by a rapid increase, followed by a gradual decrease leading up to the Pp1 acme, very rare in the acme, and sporadically reoccurring in Pp2 (Fig. 8). A very similar trend is observed at Mead, except that there is also a peak in abundance directly above the K/Pg boundary (Fig. 9). A more patchy record at mid-Waipara is consistent with the neritic setting, but here too the genus is common in the uppermost Cretaceous, declines in the basal Paleocene, and is very rare through Pp1 (Fig. 7). To explain these trends, we invoke a fall in sea level close to the K/Pg boundary, followed by a transgressive-regressive cycle that culminates in a larger fall in sea level at the time of the Pp1 acme.

678 ***Glaphyrocysta*** is interpreted to be an indicator of nearshore, high-energy conditions (Stover
679 et al., 1996; Sluijs et al., 2005; Crouch and Brinkhuis, 2005; Willumsen and Vajda, 2010a;
680 Vellekoop et al., 2015). An acme directly above the K/Pg boundary at mid-Waipara (Fig. 7) is
681 consistent with the decline in abundance of *Impagidinium,* suggesting either significant
682 shallowing or increased transport and redeposition of nearshore particles and microfossils
683 following directly after the K/Pg boundary event.

684 *4.3. Integrating temperature and environmental reconstructions*

685 The TEX_{86}-SST record from mid-Waipara River has been tied to dinoflagellate acme events
686 that can be traced from the shelf setting at mid-Waipara to the pelagic upper slope sections
687 at Branch and Mead streams (Fig. 10A-E). The cooling event (Interval III) corresponds with
688 an acme in *P. pyrophorum* that occurs at ~65.0-64.8 Ma in all three sections (Fig. 10B). The
689 underlying warming event (Interval II) is associated with a *T. evittii* acme at mid-Waipara,
690 which appears to occur directly above the K/Pg within foraminiferal zone P0. Although there
691 is no *T. evittii* acme directly above the K/Pg at Branch and Mead sections, there is and
692 increase in *Palaeocystodinium* that is consistent with warming. If these two taxa are
693 combined as a guide to warm conditions (Fig. 10C), they are in close agreement with the
694 TEX_{86} record: peaking in the earliest Paleocene, absent during the cooling event at ~65 Ma,
695 and then increasing again above this event. These taxa also provide insight into temperature
696 variation within the interval not preserved at mid-Waipara. At Branch and Mead, there is a
697 general decline in the abundance of warm-water taxa, reaching a minimum between 65.9
698 and 65.7 Ma, followed by a gradual increase and peak in *T. evittii* at ~65.2 Ma. Above this
699 peak there is a rapid decline concomitant with the increase in *P. pyrophorum*.

700 Similar trends have been observed in lithofacies changes in the pelagic K/Pg sections in
701 Marlborough (Hollis et al., 1995; 2003a, b; Hollis, 2003). In these sections, the K/Pg
702 coincides with a change from siliceous limestone to calcareous porcellanite or mudstone.
703 Within ~50 cm of the boundary, the lithology changes to chert or carbonate-poor

porcellanite. Carbonate concentration only returns to Cretaceous levels at ~64.2 Ma. Because the trend in silica is correlated with trends in siliceous microfossil abundance, both diatoms and radiolarians, the trend was interpreted as a localised response to the climate perturbations that followed the K/Pg event (Hollis, 2003; Hollis et al. 2003a, b).

A detailed record of these lithofacies changes was obtained from the Flaxbourne River and Branch Stream K/Pg boundary sections (Hollis et al., 2003a, b; Fig. 10D-E). The Flaxbourne section is the most complete K/Pg section in the South Pacific region. In addition to a well-defined iridium anomaly, it contains a full succession of foraminiferal zones from P0 to P1b (Strong et al., 1987; Strong, 2000). Unfortunately, dinoflagellates have not been recovered from this section despite extensive sampling (Willumsen, 2003). The highly siliceous Branch Stream section lacks the age control provided by foraminifera, but the expanded succession of radiolarian and dinoflagellates suggests that it is similarly complete and much more expanded, e.g. the interval to the top of radiolarian zone RP3 is ~10 m thick at Flaxbourne River but at least 55 m thick at Branch Stream.

A comparison of the lithofacies trends at the two sections with the dinoflagellate records supports inferences drawn from the lithofacies. Carbonate content decreases across the boundary at Branch Stream, recovers slightly in the earliest Paleocene and then decreases to very low levels until above the *P. pyrophorum* event. Silica content exhibits an opposite trend, except that in two intervals there is a marked increase in clay. The lower of these coincides with the *T. evittii* acme at this section and may signal increased sediment input during an interval of relative warmth. The second interval occurs within the *P. pyrophorum* acme and here may be a response to a fall in base level, linked to cooling and the unconformity at mid-Waipara. The Flaxbourne section was situated in a more distal and deeper-water setting, as evident from the weaker fluctuation in clay content. Here too, carbonate content decreases across the boundary, but remains moderately high through the earliest Paleocene before a stepped decrease at ~65 Ma. The remarkable agreement between the silica-carbonate ratio at this mid-bathyal site and the interval correlated to the *P.*

pyrophorum acme and the TEX_{86} SST minimum at mid-Waipara is compelling evidence for pronounced regional cooling in the seas offshore eastern New Zealand at this time.

4.3. Comparison with global records

Previous studies have identified a transient episode of pronounced cooling immediately following the K/Pg boundary event (Brinkhuis et al., 1998; Galleotti et al., 2004, Vellekoop et al., 2014; 2015; 2016). The lack of evidence for such a cooling event in the mid-Waipara River section is likely due to bioturbation across the boundary, which would have diluted the expression of a transient climate perturbation.

The 2.5 to 4°C warming that occurs across the K/Pg boundary at mid-Waipara represents a shift to either warm subtropical ($pTEX_{86}$) or to near tropical conditions (TEX_{86}^{H} and $BAYSPAR_{SST}$). The transient cold interval at Brazos River is followed by a similar episode of warming that spans foraminiferal zone P0 and part of Pα (Vellekoop et al., 2014). However, warming is not observed in other K/Pg boundary sections in the western Atlantic or in Tunisia (Vellekoop et al., 2015; 2016). Short-lived recovery of planktic foraminifera over an equivalent time interval at the Flaxbourne River section in Marlborough has also been cited as evidence for warming following the K/Pg event (Hollis, 2003; Hollis et al., 2003b).

The pronounced cooling within Interval III at mid-Waipara has parallels with the K/Pg boundary record on Seymour Island where cool temperatures are indicated by plant proxies (Poole et al., 2005) and clumped isotope data (Petersen et al., 2016) although the evidence from GDGT-based proxies is equivocal (Kemp et al., 2014). A weak cooling trend is also evident in TEX_{86} records from the western Atlantic K/Pg boundary sections (Vellekoop et al., 2014; 2016). Notably, these cooler temperatures span an unconformity at Brazos River, Meirs Farm and Bass River, the timing of which compares well with the unconformity at the base of Interval III at mid-Waipara. An unconformity at about this level also marks the base of the Sobral Formation on Seymour Island (Kemp et al., 2014; Witts et al., 2016).

In New Zealand, the associated acme in *P. pyrophorum* can be used to correlated Interval III at mid-Waipara to the Branch and Mead Stream sections in Marlborough (Fig. 10). The interval is centred at 65 Ma, persists for ~200 kyrs and correlates with a peak in silica concentration in the pelagic succession at Flaxbourne River (Fig. 10). This provides the first direct evidence that the marked increase in biogenic silica accumulation (diatoms and radiolarians) in these Marlborough sections during the early Paleocene was linked to pronounced cooling of surface waters and, potentially, enhanced upwelling offshore eastern New Zealand. Temperature cooled by 10-13°C between Intervals II and III and SSTs within Interval III are ~5 to 6°C cooler than average Cretaceous values. For even the warmest calibrations, SST for Interval III dropped to a minimum of ~12-14°C, which is comparable to present day temperatures for offshore southern New Zealand and implies remarkable cooling. The association of pronounced cooling and a major unconformity in a shelfal setting implies a glacio-eustatic event and the timing is consistent with the Da2 sequence boundary reported by Hardenbol et al. (1998). It is possible that the unconformity represents an amalgamation of the Da1-Da2 sequence boundary (Fig. 10).

The marine lithofacies and pollen records from New Zealand suggests the entire interval represented by the unconformity (i.e. ~66 to ~65 Ma) was cooler than the latest Maastrichtian. The interval is characterised by high silica content and abundant diatoms in the Marlborough sections (Fig. 10; Hollis et al., 1995; 2003a, b; Hollis, 2003) and in the terrestrial Moody Creek Mine section, cool temperate conifers are abundant in the pollen and spore record above the tree fern-dominated interval (Vajda et al., 2001). A recent reconstruction of pCO_2 from New Zealand Cretaceous and Paleocene sections records a fall in pCO_2 across the K/Pg boundary (Steinthorsdottir et al., 2016). The interval with low pCO_2 values is associated with early Paleocene pollen assemblages dominated by gymnosperms and with abundant *Phyllocladidites mawsonii (*Pole and Vajda, 2009*)* suggesting a correlation with Interval III at mid-Waipara.

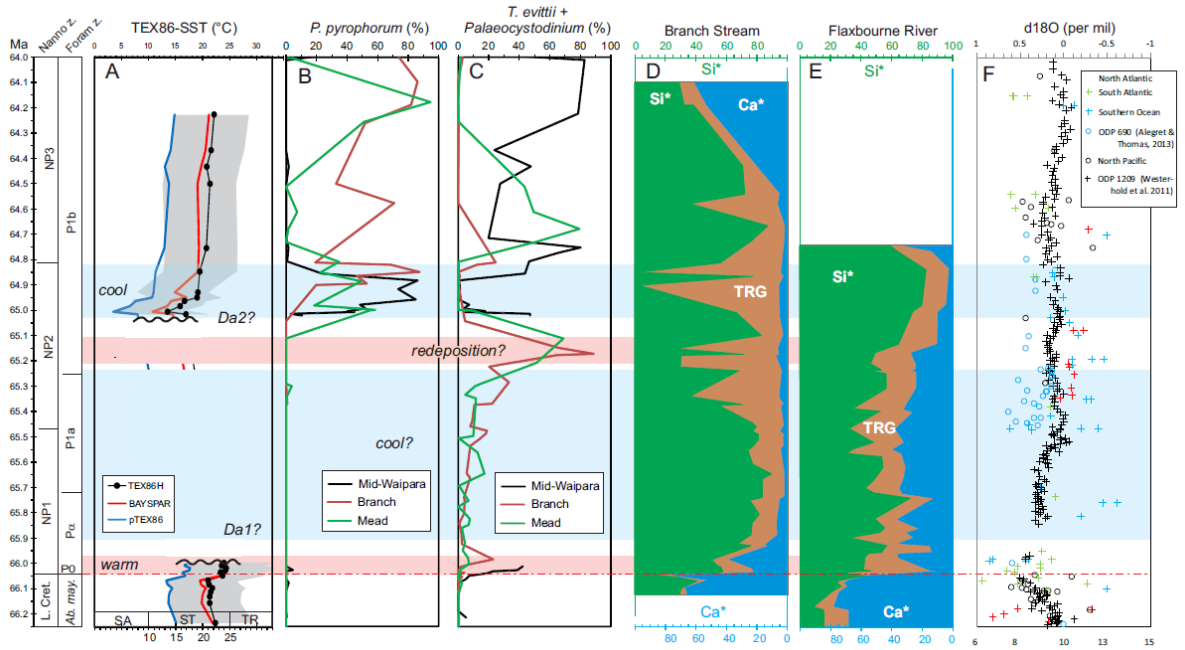

784

785 *Figure 10. Variation in climate and environmental indicators through the K/Pg transition at*
786 *mid-Waipara River (A-C), Mead Stream (B-C), Branch Stream (B-D) and Flaxbourne River*
787 *(E), together with corresponding global $\delta^{18}O$ record adapted from Zachos et al., (2008) (F).*
788 *SST estimates are derived from TEX86H, pTEX86 and BAYSPARSST calibrations, with*
789 *upper and lower 95% confidence limits for BAYSPAR also shown (grey lines). Abbreviations:*
790 *Da1, Da2 = sequence boundaries (Hardenbol et al., 1998); SA, CS, WS, Trop. =*
791 *Subantarctic, Cool Subtropical, Warm Subtropical and Tropical biogeographic zones (Nelson*
792 *and Cooke, 2001); Ca*, Si*, TRG = excess or biogenic CaCO3 and SiO2 and terrigenous*
793 *sediment, based on XRF data and the normative equations of Hollis et al. (2003a, b).*

794

795 Counter to this, pronounced early Paleocene cooling is not evident in benthic oxygen isotope
796 compilations (Zachos et al, 2008; Cramer et al. 2009, 2011), nor in a moderately high
797 resolution record from the north Pacific (Westerhold et al., 2011). We suggest that cooling
798 may have been restricted to southern high latitudes. This region is poorly represented in the
799 global compilations (Fig. 12F) and more recent datasets indicate temperatures some ~2°C
800 cooler than previously indicated (Alegret and Thomas, 2013).

4.4. Mechanisms for long-term climate impacts

Several studies have modelled the potential impacts of the K/Pg bolide impact and or Deccan Traps volcanism on the carbon cycle and climate (Caldeira and Rampino, 1990; 1993; Caldeira et al. 1990; Henehan et al. 2016; Bardeen et al. 2017; Brugger et al. 2017). The relative importance of soot, other forms of particulate dust, sulphate aerosols, CO_2 and primary production varies between these models, but all point to significant climate shifts associated with the event. The most recent modelling studies (Bardeen et al. 2017; Brugger et al. 2017) that combine the effects of soot and/or aerosols with CO_2 indicate that pronounced but short-lived cooling would have been followed by longer-lived warming. Earlier modelling experiments (Caldeira and Rampino, 1990; 1993; Caldeira et al. 1990) showed how extinctions of calcareous plankton coupled with continued supply of carbonate to the oceans would have resulted in CO_2 drawdown, climatic cooling and rapid deepening of the carbonate compensation depth (CCD). All these experiments have been based on one or at most three (where Deccan volcanism was considered) fixed-point perturbations and have not considered how the effects might be modulated by background climatic and ecological processes, such as Milankovitch cycles and post-extinction re-establishment on ecological niches. D'Hondt et al. (1996a, b; 1998) highlighted the significance of these factors by describing the dramatic change from low-amplitude precession to high-amplitude eccentricity cycles across the K/Pg boundary in addition to the delayed recovery of the pelagic ecosystem. Coxall et al. (2006) argued that full recovery of the pelagic ecosystem may have taken ~4 Myrs although a more recent study (Birch et al., 2016) suggests it may have been only 1.8 Myrs. Over approximately the same time interval, high-amplitude eccentricity cycles in carbonate flux and grain size in Walvis Ridge ODP Site 1262 indicates orbital pacing of CCD depth (Kroon et al. 2007); the inference being that each pulse of deepening is linked to CO_2 drawdown and climatic cooling. Eccentricity cycles have also been reported in the lower Paleocene sequence in Marlborough (Field and Hollis, 2003)

828 although the coeval interval in North Pacific ODP site 1209 is described as “strange interval”
829 by Westerhold et al. (2008) because it lacks coherent cycles.

830 In summary, the evidence from these modelling and proxy studies allows us to conclude that
831 a major extinction event and disruption to biogeochemical pathways plausibly explains the
832 type of long-term disruption to climate that is evident in the New Zealand K/Pg boundary
833 sections. The pronounced cooling evident in the New Zealand record has not been reported
834 in other studies, suggesting that it may be a localised response of stronger climate
835 oscillations and perhaps enhanced seasonality (D’Hondt et al., 1996). However, the absence
836 of this cooling event in global compilations of ocean temperature history (Zachos et al.,
837 2008; Cramer et al., 2009, 2011) may also be due to the patchy representation of southern
838 high-latitude climate archive (Fig. 10F).

839

840 **6. Conclusions**

841 A new TEX_{86}-based SST record across the K/Pg boundary at mid-Waipara River,
842 Canterbury Basin, New Zealand, provides long-term context for the mass extinction event
843 and oceanographic changes in the southwest Pacific from latest Cretaceous to early
844 Paleocene time (~66.2 to 64.2 Ma).

845 Bioturbation complicates the SST record across the K/Pg boundary in two respects. Firstly, a
846 down-worked GDGT assemblage is inferred to give a false indication of climatic warming
847 before the K/Pg boundary event. This inference is supported by down-working of Paleocene
848 microfossils (dinoflagellates) and siderophilic elements associated with the boundary.
849 Secondly, bioturbation has blurred the GDGT signal within the boundary zone. This means
850 that we lack a record of climatic changes precisely at the boundary.

851 Nevertheless, two significant shifts in SST are observed that can be related to regional
852 changes in oceanographic conditions and marine plankton communities as well as two

853 global climatic changes. SST warmed by ~3°C across the K/Pg boundary and then
854 remained stable for up to 40 ka (corresponding to foraminiferal zone P0). Warming was
855 associated with an influx of the warm-water dinoflagellate species, *Trithyrodinium evittii*, and
856 the short-lived recovery of calcareous-shelled plankton.

857 Following this episode of warm climatic conditions, our records reveal a period of prolonged
858 environmental instability that is manifested by a succession of short-lived acmes in
859 dinoflagellate species as well as a turnover of the assemblages from a latest Maastrichtian
860 species to early Paleocene marine flora, and the FO of a number of global dinoflagellate cyst
861 index taxa. This instability culminated in an episode of pronounced cooling, 10-13°C based
862 on TEX_{86}-based approaches, which was associated with peak biogenic silica accumulation
863 in the paleo-upwelling setting of the Marlborough K/Pg boundary sections (Hollis 2003; Hollis
864 et al. 2003a, b; Willumsen, 2003). These significant fluctuations in climatic and
865 oceanographic conditions suggest a dynamic and complex recovery to the K/Pg crisis that
866 persisted for ~1.2 Myrs in the middle to high latitude Pacific Ocean.

867

868 **Acknowledgments**

869 We thank Dr. Ian D. Bull of the Bristol Node of the Natural Environment Research Council
870 (NERC) Life Sciences Mass Spectrometry Facility for technical assistance with respect to the
871 instrumentation used for organic geochemical analysis. We thank James Eldrett, Erica Crouch
872 and an anonymous reviewer whose critical comments contributed to a much improved
873 manuscript. KWRT and RDP thank NERC for funding KWRT's PhD. CJH acknowledges the
874 GNS Science Global Change through Time Programme. RDP acknowledges the Royal
875 Society Wolfson Research Merit Award and funding from the European Research Council for
876 T-GRES (FP/2007-2013 ERC Grant Agreement number 340923).

877

878 **Supplementary Figures and Tables**

879 S1: Cross plots of trace elements at mid-Waipara River including A) Ni/Ti, B) Zn/Ti, C) Cr/Ti,
880 D) Fe/Ti.

881 S2: List of samples used in this study with position relative to K/Pg boundary. See Morgans et
882 al. (2005) for full sample list.

883 S3: Relative abundance chart for selected dinoflagellate species in mid-Waipara River section.

884 S4: Organic geochemical data for mid-Waipara River section.

885 S5: List of uppermost Cretaceous and lower Paleocene bioevents in mid-Waipara, Branch,
886 Mead and Flaxbourne K/Pg boundary sections.

887 S6: Age-depth plots for A) mid-Waipara, B) Branch, C) Mead and D) Flaxbourne K/Pg
888 boundary sections.

889 S7: Age model for the mid-Waipara section.

890

References

Alegret, L., and Thomas, E. (2013). Benthic foraminifera across the Cretaceous/Paleogene boundary in the Southern Ocean (ODP Site 690): Diversity, food and carbonate saturation. *Marine Micropaleontology* **105**: 40-51.

Askin, R. A. (1988). The palynological record across the Cretaceous-Tertiary transition on Seymour Island, Antarctica. *In:* Feldmann, R. M and. Woodbine, M. O (*Eds.)* Geology and Paleontology of Seymour Island, Antarctic Peninsula. Memoir. *Geological Society of America* **169:** 155-162

Barerra, E. and Keller, G. (1990). Stable isotope evidence for gradual environmental changes and species survivorship across the Cretaceous/Tertiary boundary. *Paleoceanography* **5**(6): 867-890

Bardeen, C. G., Garcia, R. R., Toon, O. B., and Conley, A. J. (2017). On transient climate change at the Cretaceous−Paleogene boundary due to atmospheric soot injections. *Proceedings of the National Academy of Sciences*; doi: 10.1073/pnas.1708980114

Barrera, E. and Keller, G. (1994). Productivity across the Cretaceous/Tertiary boundary in high latitudes. *Geological Society of America Bulletin* **106*:*** 1254-1266

Beerling, D. J., Lomax, B. H., Royer, D. L., Upchurch, G. R. Jr, Kump, L. R. (2002). An atmospheric *p*CO2 reconstruction across the Cretaceous-Tertiary boundary from leaf megafossils. *Proceedings of the National Academy of Sciences USA* **99:** 7836-7840.

Birch, H. S., Coxall, H. K., Pearson, P. N., Kroon, D., and Schmidt, D. N. (2016). Partial collapse of the marine carbon pump after the Cretaceous-Paleogene boundary. *Geology* **44**: 287-290.

Blaga, C. I. Reichart, G.-J. Heiri, O. Sinninghe Damsté J. S. (2009). Tetraether membrane lipid distributions in water-column particulate matter and sediments: a study of 47 European lakes along a north–south transect. *Journal of Paleolimnology* **41**: 523–540

Boersma, A and Shakleton, N. J. (1977). Tertiary oxygen and carbon isotope stratigraphy, Site 357 (mid latitude South Atlantic). *In: Initial Reports of the Deep Sea Drilling Project,* **39***.* U.S Government Printing Office, Washington D.C: 911-924

Boersma, A., Shackleton, N. J., Hall, M. A. and Given, Q. C. (1979). Carbon and oxygen isotope records at DSDP Site 384 (North Atlantic) and some Paleocene paleotemperatures and carbon isotope variations in the Atlantic Ocean. *In: Initial Reports of the Deep Sea Drilling Project* **43**: Washington (U.S. Govt. Printing Office): 695-717

Boersma, A. and Shakleton, N. J. (1981). Oxygen and carbon isotope variations and planktonic foraminifera depth habitats, Late Cretaceous to Paleocene, Central Pacific, Deep Sea Drilling Project Sites 463 and 465. *In: Initial Reports of the Deep Sea Drilling Project,* **62***.* U.S Government Printing Office, Washington D.C.: 513-526

Bowman, V. C., Francis, J. E., Riding, J. B., Hunter, S. J. and Haywood, A. M. (2012). A latest Cretaceous to earliest Paleogene dinoflagellate cyst zonation from Antarctica, and implications for phytoprovincialism in the high southern latitudes. Review of Palaeobotany and Palynology **171**, 40-56.

Bowman, V. C., Francis, J. E., Askin, R. A., Riding, J. B. and Swindles, G. T. (2014). Latest Cretaceous–earliest Paleogene vegetation and climate change at the high southern latitudes:

palynological evidence from Seymour Island, Antarctic Peninsula. Palaeogeography, Palaeoclimatology, Palaeoecology **408**, 26-47.

Brinkhuis H., Bujak J. P., Smit J., Versteegh G. J. M. and Visscher H. (1998). Dinoflagellate-based sea surface temperature reconstructions across the Cretaceous/Tertiary boundary. *Palaeogeography, Palaeoclimatology, Palaeoecology* **141:** 67-83

Brinkhuis, H., Sengers, S; Sluijs, A., Warnaar, J., Williams, G. L. (2003). Latest Cretaceous-earliest Oligocene and Quaternary dinoflagellate cysts, ODP Site 1172, East Tasman Plateau. In: Exon, NF; Kennett, JP; Malone, MJ (eds.) Proceedings of the Ocean Drilling Program, Scientific Results, College Station, TX (Ocean Drilling Program) **189:** 1-48

Brooks, R. R., Strong, C. P., Lee, J., Orth, C. J., Gilmore, J. S., Ryan, D. E., and Holzbecher, J. (1986). Stratigraphic occurrences of iridium anomalies at four Cretaceous/Tertiary boundary sites in New Zealand. *Geology (Boulder)* **14:** 727-729

Brugger, J., Feulner, G., and Petri, S. (2017). Baby, it's cold outside: Climate model simulations of the effects of the asteroid impact at the end of the Cretaceous: Geophysical Research Letters 44: 419-427.

Burgess, C. E., Pearson, P. N., Lear, C.H., Morgans, H. E. G., Handley, L., Pancost, R. D., Schouten, S. (2008). Middle Eocene climate cyclicity in the southern Pacific: implications for global ice volume*. Geology* **36:** 651–654.

Carrie, R. H., Mitchell, L. and Black, K. D. (1998). Fatty acids in surface sediments at the Hebridean shelf edge, west of Scotland. *Organic Geochemistry* **29:** 1583-1593

Caldeira, K., and Rampino, M. R., 1990, Carbon dioxide emissions from Deccan Volcanism and a K/T boundary Greenhouse Effect: Geophysical Research Letters **17**: 1299-1302.

-, 1993, Aftermath of the end-Cretaceous mass extinction: Possible biogeochemical stabilization of the carbon cycle and climate: *Paleoceanography* **8**: 515-525.

Caldeira, K., Rampino, M. R., Volk, T., and Zachos, J. C. (1990). Biogeochemical modeling at mass extinction boundaries: Atmospheric carbon dioxide and ocean alkalinity at the K/T boundary, in Kauffman, E. G., and Walliser, O. H., eds., Extinction Events in Earth History: Proceedings of the Project 216: Global Biological Events in Earth History: Berlin, Heidelberg, Springer Berlin Heidelberg, p. 333-345.

Calvert, S. E. and Pedersen, T. F. (1993). Geochemistry of Recent oxic and anoxic marine sediments: Implications for the geological record. Marine Geology **113**, 67-88.

Chenet, A.-L., Courtillot, V., Fluteau, F., Gérard, M., Quidelleur, X., Khadri, S. F. R., Subbarao, K. V., and Thordarson, T., 2009, Determination of rapid Deccan eruptions across the Cretaceous-Tertiary boundary using paleomagnetic secular variation: 2. Constraints from analysis of eight new sections and synthesis for a 3500-m-thick composite section: Journal of Geophysical Research: Solid Earth **114** (B6); doi: 10.1029/2008JB005644

Courtillot, V., Feraud, G., Maluski, H., Vandamme, D., Moreau, M. G. and Besse, J. (1988). Deccan flood basalts and the Cretaceous/Tertiary boundary. *Nature* **333**: 843-846.

Coxall, H. K., D'Hondt, S., and Zachos, J. C. (2006). Pelagic evolution and environmental recovery after the Cretaceous-Paleogene mass extinction: Geology **24:** 297-300.

971 Claustre, H., Marty, J., Cassiani L. and Dagaut, J. (1989). Fatty acid dynamics in phytoplankton and
972 microzooplankton communities during a spring bloom in the coastal Ligurian Sea: ecological
973 implications. *Marine Microbial Food Webs* **3:** 51–66.
974 Cramer, B. S., Miller, K. G., Barrett, P. J., and Wright, J. D. (2011). Late Cretaceous-Neogene trends
975 in deep ocean temperature and continental ice volume: Reconciling records of benthic
976 foraminiferal geochemistry (d18O and Mg/Ca) with sea level history. *Journal of Geophysical*
977 *Research – Oceans* **116**: C12023.
978 Cramer, B. S., Toggweiler, J. R., Wright, J. D., Katz, M. E., and Miller, K. G. (2009). Ocean
979 overturning since the Late Cretaceous: Inferences from a new benthic foraminiferal isotope
980 compilation: *Paleoceanography* **24**: PA4216.
981 Cranwell, P. A., Eglinton, G. and Robinson, N. (1987). Lipids of aquatic organisms as potential
982 contributors to lacustrine sediments-II. *Organic Geochemistry* **11:** 513-527
983 Crouch, E. M. and Brinkhuis, H. (2005). Environmental change across the Paleocene-Eocene
984 transition from eastern New Zealand: a marine palynological approach. *Marine*
985 *micropaleontology,* **56(3/4):** 138-160
986 Crouch, E. M., Willumsen, P. S., Kulhanek., D. K., and Gibbs., S. J. (2014). A Revised Palaeocene
987 (Teurian) Dinoflagellate Cyst Zonation from Eastern New Zealand. *Review of Palaeobotany*
988 *and Palynology* **202:** 47-49
989 D'Hondt, S., King, J. and Gibson, C. (1996). Oscillatory marine response to the Cretaceous-Tertiary
990 impact. *Geology (Boulder)* **24:** 611-614
991 D'Hondt, S., Donaghay, P., Zachos, J. C., Luttenberg, D., and Lindinger, M. (1998). Organic carbon
992 fluxes and ecological recovery from the Cretaceous-Tertiary mass extinction, *Science* **282:**
993 276-279
994 Dale B. (1996). Dinoflagellate cysts ecology: modelling and geological applications. *In:* Jansonius J.,
995 McGregor D.C., (eds). Palynology: Principles and Applications. *American Association of*
996 *Stratigraphic Palynologists Foundation; Dallas*. pp. 1249–1276.
997 Dean, R. A. and Whitehead, E. V. (1961). The Occurrence of Phytane in Petroleum. *Tetrahedron*
998 *Letters:* 768-770
999 De Rosa, M., Gambacorta, A., Nicolous, B. and Bu'Lock, J. D. (1980). Complex lipids of Caldariella
1000 acidophila, a thermoacidophile archaebacterium. *Phytochemistry*. **19:** 821-825
1001 Douglas, R. G. and Savin, S. M. (1971). Isotopic analysis of planktonic foraminifera from the Cenozoic
1002 of the Northwest Pacific Leg 6. (*In*): *Initial Reports of the Deep Sea Drilling Project,* **6***.* U.S
1003 Government Printing Office, Washington, D.C.: 1123-1127
1004 Drugg, W. S. (1967). Palynology of the Upper Moreno Formation (Late Cretaceous-Paleocene)
1005 Escarpado Canyon, California. *Palaeontograpbic* **B120**: 1-71.
1006 Edwards, A. R. (1965).Calcareous nannoplankton from the uppermost Cretaceous and lowermost
1007 Tertiary of the Mid-Waipara section, South Island, New Zealand. New Zealand Journal of
1008 Geology and Geophysics **9:** 481-490.
1009 Eglinton, G. and Hamilton, R. J. (1963). The distribution of n-alkanes. *In:* Swain, T. (*ed*.), Chemical
1010 Plant Taxonomy. Academic Press, London: 87-217

1011 Eglinton, G. and Hamilton, R. J. (1967). Leaf epicuticular waxes. *Science* **156:**1322-1335.
1012 Elliot, D. H., Askin, R.A., Kyte, F. T. and Zinsmeister, W. J. (1994) Iridium and dinocysts at the
1013 Cretaceous-Tertiary boundary on Seymour Island, Antarctica: Implications for the K-T event.
1014 Geology **22:** 675-678.
1015 Evitt, W. R, Damassa, S. P., Albert, R. N. (1998). A tiger by the tail: The exophragm of the
1016 Cretaceous-Paleocene dinoflagellate Palaeoperidinium and its implications. Palynology **22:** 1-
1017 58.
1018 Fensome, R. A., Taylor, F. J. R., Norris, G., Sarjeant, W. A. S., Wharton, D. I. and Williams, G. L.
1019 (1993). A classification of living and fossil dinoflagellates. *Micropaleontology Special*
1020 *Publication* **7:** 351 pp.
1021 Ferrow, E., Vajda, V., Bender Koch, C., Peucker-Ehrenbrink, B. and Willumsen, P. S. (2011).
1022 Multiproxy analysis of a new terrestrial and a marine Cretaceous–Paleogene (K/Pg) boundary
1023 site from New Zealand. Geochimica et Cosmochimica Acta **75:** 657-672.
1024 Field, B. D., and Hollis, C. J. (2003). Orbitally controlled cyclicity around the Cretaceous-Cenozoic
1025 boundary, Marlborough, New Zealand. *New Zealand Journal of Geology and Geophysics* **46**:
1026 235-241.
1027 Field, B. D., Browne, G. H., Davy, B. W., Herzer, R. H., Hoskins, R. H., Raine, J. I., Wilson, G. J.,
1028 Sewell, R. J., Smale, D. and Watters, W. A. (1989). Cretaceous and Cenozoic sedimentary
1029 basins and geological evolution of the Canterbury region, South Island, New Zealand. New
1030 Zealand Geological Survey, Lower Hutt.
1031 Foreman., H. (1968). Upper Maestrichtian Radiolaria, leg 7, DSDP. *In:* Winterer et al. (eds). Initial
1032 Reports of the Deep Sea Drilling Project **7**. U.S. Government Printing Office, Washington: pp.
1033 407-471.
1034 Galeotti, S., Brinkhuis, H. and Huber, M. (2004). Records of a post-Cretaceous-Tertiary boundary
1035 millennial scale cooling from the western Tethys: a smoking gun for the impact-winter
1036 hypothesis? *Geological Society of America* **32**(6): 529-532
1037 Gillan, F. T., Hogg, R. W. and Drew, E. A. (1984). The sterol and fatty acid compositions of seven
1038 tropical seagrasses from North Queensland, Australia. *Phytochemistry* **23:** 2817– 2821.
1039 Gliozzi, A., Paoli, G., DeRosa, M. and Gambacorta, A. (1983). Effect of isoprenoid cyclization on the
1040 transition temperature of lipids in thermophilic archaeabacteria. *Biochimica et Biophysica Acta*
1041 **735:** 234-242
1042 Gradstein F. M., Ogg, J. G., and Hilgen., F. J. (2012). On the Geologic Time Scale. *Newsletters on*
1043 *Stratigraphy* **45**: 171–188.
1044 Habib, D. and Saeedi, F. (2007). The *Manumiella seelandica* global spike: cooling during regression
1045 at the close of the Maastrichtian, *Palaeogeography, Palaeoclimatology,* Palaeoecology **255:**
1046 87–97.
1047 Habib, D., Eshet, Y.,Van Pelt, R. (1994). In: Traverse, A. (eds), Palynology of sedimentary cycles,
1048 Sedimentation of Organic Particles, 311-335.
1049 Hardenbol, J., Thierry, J., Farley, M. B., T. Jacquin, de Graciansky, P-C. and Vail, P. R. (1998).
1050 Mesozoic and Cenozoic sequence chronostratigraphic framework of European basins, *in:* P-C.

de Graciansky *et al. [eds],* Mesozoic and Cenozoic Sequence Stratigraphy of European Basins, Spec. Publ. SEPM Soc. Sediment. *Geology* **60:** 3–13.

Harwood, D. M. (1988). Upper Cretaceous and Lower Paleocene diatom and silicoflagellate biostratigraphy of Seymour Island, eastern Antarctic Peninsula. In: R. M. Feldmann and M. O. Woodburne, eds., Geology and Paleontology of Seymour Island, Antarctic Peninsula. *Geological Society of America Memoir* **169**: 55–129.

Helby, R., Morgan, R., Partridge, A. D., (1987). A palynological zonation of the Australian Mesozoic. In: Jell, P.A. (eds) Studies in Australian Mesozoic Palynology. Memoir Association Australasian Palaeontologists 4, 1-94Heilmann-Clausen, C. (1985). Dinoflagellate stratigraphy of the uppermost Danian to Ypresian in the Viborg I borehole, central Jylland, Denmark. Danmarks *Geologiske Undersøgelse, Serie A* **7**, p.1-69, pl.1-15.

Henehan, M. J., Hull, P. M., Penman, D. E., Rae, J. W. B., and Schmidt, D. N. (2016). Biogeochemical significance of pelagic ecosystem function: an end-Cretaceous case study: *Philosophical Transactions of the Royal Society B: Biological Sciences* **371** (1694); doi: 10.1098/rstb.2015.0510

Hernandez-Sanchez., M. T., Woodward., E. M. S., Taylor., K. W. R., Henderson., G. M., and Pancost., R. D. (2014). Variations in GDGT distributions through the water column in the South East Atlantic Ocean. *Geochimica et Cosmochimica Acta* **132:** 337-348

Ho, S. L and Laepple, T. (2016). Flat meridional temperature gradient in the early Eocene in the subsurface rather than surface ocean. *Nature Geoscience* **9:** 606–610

Hollis, C. J. (2003). The Cretaceous/Tertiary boundary event in New Zealand: profiling mass extinction. *New Zealand Journal of Geology and Geophysics* **46:** 307-321

Hollis, C. J., Handley, L., Crouch, E. M., Morgans, H. E. G., Baker, J. A., Creech, J., Collins, K. S., Gibbs, S. J., Huber, M., Schouten, S., Zachos, J. C. and Pancost, R. D. (2009). Tropical sea temperatures in the high-latitude South Pacific during the Eocene. *Geology* **37:** 99-102.

Hollis, C. J., Rodgers, K. A. and Parker, R. J. (1995). Siliceous plankton bloom in the earliest Tertiary of Marlborough, New Zealand. *Geology (Boulder)* **23:** 835-838

Hollis, C. J., Rodgers, K.A., Strong, C. P., Field, B. D. and Rodgers, K. M. (2003a). Paleoenvironmental changes across the Cretaceous/Tertiary boundary in the northern Clarence Valley, southeastern Marlborough, New Zealand. *New Zealand Journal of Geology and Geophysics* **46:** 209–234

Hollis, C. J., Rodgers, K. A., Field, B. D., Strong, C. P. and Rodgers, K. M. (2003b). paleoenvironmental changes across the Cretaceous/Tertiary boundary at Flaxbourne River and Woodside Creek, eastern Marlborough, New Zealand. *New Zealand Journal of Geology and Geophysics* **46:** 177–198

Hollis, C. J. and Strong, C. P. (2003). Biostratigraphic review of the Cretaceous/Tertiary boundary transition, mid-Waipara River section, North Canterbury, New Zealand. *New Zealand Journal of Geology and Geophysics* **46:** 243-253

Hollis, C. J., Taylor, K. W. R., Handley, L., Pancost, R. D., Schouten, S., Pearson, P. N., Creech, J. B., Zachos, J. C., Gibbs, S., Crouch, E. M., Morgans, H. E. G., Crampton, J. S. and Huber, M.

(2012). Southwest Pacific marine temperature variation from Late Paleocene to Middle Eocene. *Earth and Planetary Science Letters* **349-350:** 53-66

Hopmans, E. C., Weijers, J. W. H., Schefuß, E., Herfort, L., Sinninghe Damsté, J. S., Schouten, S. (2004). A novel proxy for terrestrial organic matter in sediments based on branched and isoprenoid tetraether lipids. *Earth and Planetary Science Letters* **224:** 107–116.

Hsü, K. J., and McKenzie, J. A. (1985). A 'strangelove' ocean in the earliest Tertiary *in* E. T. Sundquist and W. S. Broecker *(eds,)* The Carbon Cycle and Atmospheric CO2: Natural Variations, Archean to Present. AGU, Washington, D. C. *Geophysical Monograph Series* **32**: 487–492

Huber, M., Caballero, R. (2011). The early Eocene equable climate problem revisited. *Climate of the Past* **7:** 241–304.

Huguet, C., Hopmans, E. C., Febo-Ayala, W., Thompson, D. H., J. S., Sinninghe Damsté, and Schouten S. (2006). An improved method to determine the absolute abundance of glycerol dibiphytanyl glycerol tetraether lipids. *Organic Geochemistry* **37:** 1036–1041.

Inglis., G. N., Farnsworth, A., Lunt, D., Foster, G., Hollis, C. J., Pagani, M., Jardine, P. E., Pearson, P. N., Markwick, P., Galsworthy, A. M. J., Raynham, L., Taylor, K. W. R., and Pancost, R. D. (2015). Descent toward the icehouse: Eocene sea surface cooling inferred from GDGT distributions. *Paleoceanography* **29:** doi:10.1002/2014PA002723

Kemp, D. B., Robinson, S.A., Crame, J. A., Francis, J. E., Ineson, J., Whittle, R. J., Bowman, V. and O'Brien, C. (2014). A cool temperate climate on the Antarctic Peninsula through the latest Cretaceous to early Paleogene. Geology **42:** 583-586.

Kim, J.-H., Schouten, S., Hopmans, E. C., Donner, B., Sinninghe Damsté, J. S. (2008). Global sediment core-top calibration of the TEX86 paleothermometer in the ocean. *Geochimica et Cosmochimica Acta* **72:** 1154–1173

Kim, J.-H., van der Meer, J., Schouten, S., Helmke, P., Willmott, V., Sangiorgi, F., Koc, N., Hopmans, E. C. and Sinninghe Damsté, J. S. (2010). New indices and calibrations derived from the distribution of crenarchaeal isoprenoid tetraether lipids: Implications for past sea surface temperature reconstructions, *Geochimica et Cosmochimica Acta*, **74**: 4639–4654

Kim, J.-H., Schouten, S., Rodrigo-Gámiz, R., Rampen, S., Marino, G., Huguet, C., Helmke, P., Buscaldi, R., Hopmans, E. C., Pross, J., Sangiorgi, F., Middelburg., J. B. M., and Sinninghe Damsté, J. S. (2015). Influence of deep-water derived isoprenoid tetraether lipids on the TEX_{86}^{H} paleothermometer in the Mediterranean Sea. *Geochmica et Cosmochimica Acta* **150**: 125-141

Keller, G. and Benjamini, C. (1991). Paleoenvironment of the eastern Tethys in the Early Paleocene. *Palaios* **6:** 439-464

Keller, G., and Lindinger, M. (1989). Stable Isotope, TOC and CaCO3 record across the Cretaceous/Tertiary Boundary at El Kef, Tunisia, Paleogeography, Paleoclimatology, Paleoecology, **73**(3/4): 243-265

Koch, B. P., Rullkötter, J. and Lara, R. J. (2003). Evaluation of triterpenols and sterols as organic matter biomarkers in a mangrove ecosystem in northern Brazil. *Wetlands Ecology and Management* **11:** 257–263.

Kring, D. A. (2007). The Chicxulub impact event and its environmental consequences at the Cretaceous-Tertiary boundary. *Palaeogeography, Palaeoclimatology, Palaeoecology* **255***:* 4-21

Kroon, D., Zachos J.C., and Leg 208 Scientific Party (2007). Leg 208 synthesis: Cenozoic climate cycles and excursions, Proceedings of ODP, Scientific Results 208, College Station, TX. 1–55

Köthe, A. (1990). Paleogene dinoflagellates from Northwest Germany: biostratigraphy and paleoenvironments. Geologisches Jahrbuch, Reihe A, Heft 118, 3-111

Lengger, S. K., Hopmans, E. C., Reichart, G.-J., van Nierop, K. G. J., Sinninghe Damsté, J. S., and Schouten, S. (2012). Distribution of core and intact polar glycerol dibiphytanyl glycerol tetraether lipids in the Arabian Sea oxygen minimum zone. II: Evidence for selective preservation and degradation in sediments and consequences for the TEX86. *Geochimica et Cosmochimica Acta* **98**: 244–258

Magaritz, M., Benjamini, C., Keller, G. and Moshkovitz, S. (1992). Early diagenetic isotopic signal at the Cretaceous/Tertiary boundary, Israel. *Palaeogeography, Palaeoclimatology, Palaeoecology* **91**: 291–304

Nøhr-Hansen H. and Dam G. (1997). Palynology and sedimentology across a new marine Cretaceous/Tertiary boundary section on Nuussuaq, West Greenland. *Geology* **25:** 851-854

Nøhr-Hansen, H., Dam, G. (1999). Emendation of Trithyrodinium evittii Drugg 1967 and Trithyrodinium fragile Davey 1969 an artificial split of one dinoflagellate cyst species - Stratigraphic and paleoenvironmental importance. Grana **138:** 125-133

Morgans, H. E. G., Jones, C.M., Crouch, E. M., Field, B. D., Hollis, C.J., Raine, I. J., Strong, C. P., and Wilson, G. J. (2005). Upper Cretaceous to Eocene stratigraphy and sample collections, mid-Waipara River section, North Canterbury. *Institute of Geological and Nuclear Sciences, Science Report* **2003/08:** 101 pp.

Oberhänsli, H. (1986). Latest Cretaceous-Early Neogene oxygen and carbon isotope record as DSDP sites in the Indian Ocean. *Marine Micropaleontology* **10**(1-3): 91-116

Pancost, R. D., Taylor, K. W. R., Inglis, G. N., Kennedy, E. M., Handley, L., Hollis, C. J., Crouch, E. M., Huber, M., Schouten, S., Pearson, P. N., Mogans, H. E. G., Raine, J. I. (2013). *Geochemistry, Geophysics, Geosystems,* **14(2):** pp. 5413-5429

Pearson, P. N., Ditchfield, P., Singano, J., Harcourt-Brown, K., Nicholas, C., Olsson, R., Shackleton, N. J., Hall, M. (2001). Warm tropical sea surface temperatures in the Late Cretaceous and Eocene epochs. *Nature* **413**: 481–487.

Pearson, P. N., van Dongen, B. E., Nicholas, C. J., Pancost, R.D., Schouten, S., Singano, J. M., Wade, B. S. (2007). Stable warm tropical climate through the Eocene Epoch. *Geology* **35:** 211–214.

Petersen, S. V., Dutton, A. and Lohmann, K. C. (2016). End-Cretaceous extinction in Antarctica linked to both Deccan volcanism and meteorite impact via climate change. Nature Communications **7:** doi:10.1038/ncomms12079.

1171 Pierazzo, E., Kring, D. A. and Melosh, H. J. (1998). Hydrocode simulation of the Chicxulub impact
1172 event and the production of climatically active gases. *Journal of Geophysical Research* **103:**
1173 28607–28625.
1174 Pierazzo, E., Hahmann, A. N. and Sloan, L. C. (2003). Chicxulub and Climate: Radiative Pertubations
1175 of Impact-Produced S-Bearing Gases. *Astrobiology* **3:** 99-118
1176 Pole, M. and Vajda, V. (2009). A new terrestrial Cretaceous-Paleogene site in New Zealand—
1177 turnover in macroflora confirmed by palynology. *Cretaceous Research* **30:** 917-938.
1178 Pope, K. O., Baines., K. H., Ocampo, A. C. and Ivanov, B. (1994). Impact winter and the Cretaceous
1179 Tertiary extinctions: Results of a Chicxulub asteroid impact model. *Earth and Planetary*
1180 *Science Letters* **128:** 719-725
1181 Pope, K. O, Baines, K. H., Ocampo, A. C. and Ivanov, B. (1997). Energy, volatile production, and
1182 climate effects of the Chicxulub Cretaceous/Tertiary impact. *Journal of Geophysical Research*
1183 **102:** 21,645-21,664
1184 Rampino, M. R. and Stothers, R. B. (1988). Flood basalt volcanism during the past 250 million years.
1185 *Science* **241:** 663 – 668
1186 Robinson, N., Eglinton, G., Brassell, S. C. and Cranwell, P.A. (1984). Dinoflagellate origin for
1187 sedimentary 4α-methylsteroids and 5α(H)-stanols. Nature **308**: 439–442.
1188 Rontani, J. F. and Volkman, J. K. (2003). Phytol degradation products as biogeochemical
1189 tracers in aquatic environments. *Organic Geochemistry* **34:** 1-35.
1190 Schoene, B., Samperton, K. M., Eddy, M. P., Keller, G., Adatte, T., Bowring, S.A., Khadri, S. F. R. and
1191 Gertsch, B. (2015) U-Pb geochronology of the Deccan Traps and relation to the end-
1192 Cretaceous mass extinction. *Science* **347**: 182-184.
1193 Schouten, S., van der Meer, M. J. T., Hopmans, E. C. and Sinninghe Damsté, J. S. (2007). Archaeal
1194 and bacterial glycerol dialkyl glycerol tetraether lipids in hot springs of Yellowstone National
1195 Park. *Applied and Envrionmental Microbiology* **73:** 6181-6191
1196 Schouten, S., Pitcher, A., Hopmans, E. C., Villanueva, L., van Bleijswijk, J., and Sinninghe Damsté, J.
1197 S. (2012). Distribution of core and intact polar glycerol dibiphytanyl glycerol tetraether lipids in
1198 the Arabian Sea oxygen minimum zone: I: selective preservation and degradation in the water
1199 column and consequences for the TEX86. *Geochimica et Cosmochimica Acta*, **98**: 228–243
1200 Schouten, S., Hopmans, E. C., Schefuß, E. and Sinninghe Damsté, J.S. (2002). Distributional
1201 variations in marine crenarchaeotal membrane lipids: a new tool for reconstructing ancient sea
1202 water temperatures? *Earth and Planetary Science Letters* **204:** 265-274.
1203 Schouten, S., Hopmans, E. C. and Sinninghe Damsté, J. S. (2013). The organic geochemistry of
1204 glycerol dialkyl glycerol tetraether lipids: a review. *Organic Geochemistry* **54:** 19-61
1205 Schulte, P., Alegret, L., Arenillas, I., Arz, J. A.,. Barton, P. J., Bown, P. R., Bralower, T. J., Christeson,
1206 G. L., Claeys, P., Cockell, C. S., Collins, G. S., Deutsch, A., Goldin, T. J., Goto, K., Grajales-
1207 Nishimura, J. M., Grieve, R. A. F., Gulick, S. P. S., Johnson, K. R., Kiessling, W., Koeberl, C.,
1208 Kring, D. A., MacLeod, K. G., Matsui,T., Melosh, J., Montanari, A., Morgan, J. V., Neal, C. R.,
1209 Nichols, D. J., Norris, R. D., Pierazzo, E., Ravizza, G., Rebolledo-Vieyra, M., Uwe Reimold,
1210 W., Robin, E., Salge, T., Speijer, R. P., Sweet, A. R., Urrutia-Fucugauchi, J., Vajda, V.,

Whalen, M. T., and Willumsen, P. S. (2010). The Chicxulub asteroid impact and mass extinction at the Cretaceous- Paleogene Boundary. *Science* ***327***: 1214–1218

Self, S., Schmidt, A. and Mather, T. A. (2014). Emplacement characteristics, time scales, and volcanic gas release rates of continental flood basalt eruptions on Earth. *Geological Society of America Special Papers* ***505***, doi:10.1130/2014.2505(1116).

Sluijs, A., Pross, J. and Brinkhuis, H. (2005). From greenhouse to icehouse; organic-walled dinoflagellate cysts as paleoenvironmental indicators in the Paleogene. Earth-Science Reviews **68:** 281-315.

Serrazanetti, G. P., Folicaldi, A., Guerrini, F., Monti, G., Pistocchi, R. and Boni, L. (2006). Microalgal lipid markers for palaeoclimate research. Climate Research **31:** 145-150

Sexton, P.F., Wilson, P.A., Pearson, P.N. (2006). Microstructural and geochemical perspectives on planktic foraminiferal preservation: "Glassy" versus "Frosty. *Geochemistry, Geophysics, Geosystems* **7:** Q12P19

Shimada, H., Nimoto, N., Shida, Y., Oshima, T. and Yamagishi, A. (2002). Complete polar lipid composition of *Thermoplasma acidophilum* HO-62 determined by High-Performance Liquid Chromatography with Evaporative Light-Scattering Detection. *Journal of Bacteriology* **184**(2): 556-563

Steinthorsdottir, M., Vajda, V. and Pole, M. (2016). Global trends of pCO2 across the Cretaceous–Paleogene boundary supported by the first Southern Hemisphere stomatal proxy-based pCO2 reconstruction. *Palaeogeography, Palaeoclimatology, Palaeoecology* **464: 143-152;**

Stover, L.E., Brinkhuis, H., Damassa, S. P., de Verteuil, L., Helby, R. J., Monteil, E., Partridge, A. D., Powell, A. J., Riding, J. B., Smelror, M., and Williams, G. L. (1996). Mesozoic–Tertiary dinoflagellates, acritarchs and prasinophytes. In: Jansonius, J. & McGregor, D.C. (Eds), Palynology: Principles and applications, 2. American Association of Stratigraphic Palynologists Foundation, Dallas, Texas, 641–750

Stott, L. D., and Kennett, J. P. (1990). The paleoceanographic and paleoclimatic signature of the Cretaceous/Paleogene boundary in the Antarctic: stable isotopic results from ODP Leg 113. *In* Barker, P.F., Kennett, J.P., et al., *Proceedings of the Ocean Drilling Program, Scientific Results* 113**:** College Station, TX (Ocean Drilling Program) 829–848

Strong, C. P. (1977). Cretaceous-Tertiary boundary at Woodside Creek, north-eastern Marlborough. *New Zealand Journal of Geology and Geophysics* **20:** 687-696

Strong, C. P. (1984). Cretaceous–Tertiary boundary, mid-Waipara River section, North Canterbury, New Zealand. *New Zealand Journal of Geology and Geophysics* **27:** 231–234

Strong, C. P. (2000). Cretaceous-Tertiary foraminiferal succession at Flaxbourne River, Marlborough, New Zealand. *New Zealand Journal of Geology and Geophysics* **43:** 1-20

Strong, C. P., Brooks, R.R., Orth, C.J. and Xueying, M. (1988). An iridium-rich calcareous claystone (Cretaceous-Tertiary boundary) from Wharanui, Marlborough, New Zealand. *New Zealand Journal of Geology and Geophysics* **31**: 191-195

1249 Strong, C. P., Brooks, R. R., Wilson, S. M., Reeves, R. D., Orth, C. J., Mao, X.-Y., Quintana, L. R. and
1250 Anders, E. (1987). A new Cretaceous-Tertiary boundary site at Flaxbourne River, New
1251 Zealand; biostratigraphy and geochemistry. *Geochimica et Cosmochimica Acta* **51:** 2769-2777
1252 Taylor, K. W. R., Huber., M., Hollis., C. J., Hernandez-Sanchez., M. T., and Pancost., R. D. (2013).
1253 Re-evaluating modern and Palaeogene GDGT distributions: Implications for SST
1254 reconstructions. *Global and Planetary Change* **108:** 158 - 174
1255 Tierney, J. E. and Tingley, M. P. (2015). A TEX86 surface sediment database and extended Bayesian
1256 calibration. *Scientific Data* **2:** 150029
1257 Turich, C., Freeman, K. H., Bruns, M. A., Conte, M., Jones, A.D., Wakeham, S. G. (2007). Lipids of
1258 marine archaea: patters and provenance in the water-column and sediments. *Geochimica et*
1259 *Cosmochimica Acta* **71:** 3272–3291.
1260 Uda, I., Sugai, A., Itoh, Y. H., and Itoh, (2001). T. Variation on molecular species of polar lipids from
1261 *Thermoplasma acidophilum* depends on growth temperature. *Lipids* **36:** 103-105.
1262 Vajda, V. and Raine, J. I. (2003). Pollen and spores in marine Cretaceous/Tertiary boundary
1263 sediments at mid-Waipara River, North Canterbury, New Zealand, *New Zealand Journal of*
1264 *Geology and Geophysics* **42:** 255-273
1265 Vajda, V., Raine, J. I., and Hollis, C. J. (2001). Indication of global deforestation at the Cretaceous–
1266 Tertiary boundary by New Zealand fern spike. *Science* **294:** 1700-1702.
1267 Vellekoop, J., Sluijs, A., Smit, J., Schouten, S., Weijers, J.W.H., Sinninghe Damsté, J.S. and
1268 Brinkhuis, H. (2014). Rapid short-term cooling following the Chicxulub impact at the
1269 Cretaceous–Paleogene boundary. *Proceedings of the National Academy of Sciences:* doi:
1270 10.1073/pnas.1319253111.
1271 Vellekoop, J., Smit, J., van de Schootbrugge, B., Weijers, J.W.H., Galeotti, S., Sinninghe Damsté,
1272 J.S. and Brinkhuis, H. (2015). Palynological evidence for prolonged cooling along the Tunisian
1273 continental shelf following the K/Pg boundary impact. *Palaeogeography, Palaeoclimatology,*
1274 *Palaeoecology* **426**: 216-228.
1275 Vellekoop, J., Esmeray-Senlet, S., Miller, K. G., Browning, J. V., Sluijs, A., van de Schootbrugge, B.,
1276 Sinninghe Damsté, J. S., and Brinkhuis, H. (2016). Evidence for Cretaceous-Paleogene
1277 boundary bolide “impact winter” conditions from New Jersey, USA. *Geology*, **44**: 619-622; doi:
1278 10.1130/G37961.1
1279 Versteegh, G. J. M., Schefuß, E., Dupont, L., Marret, F., Sinninghe-Damsté, J. S., Jansen, J. H. F.
1280 (2004). Taraxerol and Rhizophora pollen as proxies for tracking past mangrove ecosystem.
1281 *Geochimica et Cosmochimica Acta* **68:** 411–422.
1282 Villanueva, L., Schouten, S., and Sinninghe-Damsté, J. S. (2015). Depth-related distribution of a key
1283 gene of the tetraether lipid biosynthetic pathway in marine Thaumarchaeota. *Environmental*
1284 *Microbiology* **10:** 3527-3539
1285 Volkman, J. K. (2003). Sterols in microorganisms. *Applied Microbiology and Biotechnology* **60**: 495-
1286 506

Volkman, J. K., Johns, R. B., Gillian, F. T., Perry, G. J. and Bavor, H. J. Jr. (1980). Microbial lipids of an intertidal sediment 1: Fatty acids and hydrocarbons. *Geochimica et Cosmochimica Acta* **44**: 1133-1143.

Volkman J. K., Kearney, P., and Jeffrey, S. W. (1990). A new source of 4-methyl sterols and 5α(H)-stanols in sediments: Prymnesiophyte microalgae of the genus Pavlova. *Organic Geochemistry* **15**: 489–497.

Volkman, J. K., Barrett, S. M., Dunstan, G. A. and Jeffrey, S. W. (1993). Geochemical significance of the occurrence of dinosterol and other 4-methyl sterols in a marine diatom. *Organic Geochemistry* **20**: 7–16.

Volkman J. K., Barrett S. M., Blackburn S. I., Mansour M. P., Sikes E. L. and Gelin F. (1998). Microalgal biomarkers: a review of recent research developments. *Organic Geochemistry* **29**: 1163–1179.

Wannigama, G. P., Volkman, J. K., Gillan, F. T., Nichols, P. D. and Johns, R. B. (1981). A comparison of lipid components of the fresh and dead leaves and pneumatophores of the mangrove Avicennia marina. *Phytochemistry* **20:** 659–666

Weijers,, J. W. H., Schouen, S., Spaargaren, O. C. and Sinninghe Damsté, J.S. (2006). Occurrence and distribution of tetraether membrane lipids in soils: implication for the use of the TEX_{86} proxy and the BIT index. *Organic Geochemistry* **37**: 1680-1693

Westerhold, T., Röhl, U., Raffi, I., Fornaciari, E., Monechi, S., Reale, V., Bowles, J., and Evans, H. F. (2008). Astronomical calibration of the Paleocene time. *Palaeogeography, Palaeoclimatology, Palaeoecology* **257**: 377-403.

Westerhold, T., Röhl, U., Donner, B., McCarren, H. K. and Zachos, J. C. (2010). A complete high-esolution benthic stable isotope record for the central Pacific (ODP Site 1209). *Paleoceanography* **26:** PA2216

Wilf, P., Johnson, K. R., and Huber, B. T. (2003). Correlated terrestrial and marine evidence for global climate changes before mass extinction at the Cretaceous–Paleogeneboundary, P*roccedings of the* N*ational* A*cademy of* S*cience* **100:** 599-604

Wilson, G. J. (1987). Dinoflagellate biostratigraphy of the Cretaceos-Tertiary boundary, mid-Waipra River Section, North Canterbury, New Zealand. Geological Survey Record **20:** 8-16.

Willumsen, P. S. (2003). Marine Palynology across the Cretaceous-Tertiary Boundary in New Zealand: PhD thesis, Victoria University of Wellington

Willumsen, P. S. (2004). Two new species of the dinoflagellate cyst genus *Carpatella* Grigorovich 1969 from the Cretaceous-Tertiary transition in New Zealand. Journal of Micropalaeontology **23:** 119–125.

Willumsen, P. S (2006). *Palynodinium minus* sp. nov., a new dinoflagellate cyst from the Cretaceous/Paleogene transition in New Zealand; its significance and palaeoecology. *Cretaceous Research* **27:** 954-963

Willumsen, P. S. (2011). Maastrichtian to Paleocene dinocysts from the Clarence Valley, South Island, New Zealand. *Alcheringa: An Australasian Journal of Palaeontology* **35:** 199-240

1326 Willumsen, P. S. (2012). Three new species of dinoflagellate cysts from Cretaceous-Paleogene
1327 boundary transitions at mid-Waipara River and Fairfield Quarry, South Island, New Zealand.
1328 Palynology **36:** 48-62. DOIdoi:10.1080/01916122.2011.642260
1329 Willumsen, P. S., Vajda, V. (2010a). A new early Paleocene dinoflagellate cyst species,
1330 *Trithyrodinium partridgei*; Its biostratigraphic significance and palaeoecology. Alcheringa **34**
1331 **(4):** 523–538. DOI: 10.1080/03115518.2010.519258.
1332 Willumsen, P. S., Vajda, V. (2010b). Ecosystems response and restitution time across the K/Pg
1333 boundary transition at high-latitudes, Southern Hemisphere, New Zealand – a palynological
1334 approach. Geophysical Research Abstracts, Vol. 12, EGU2010-11379, EGU General
1335 Assembly 2010
1336 Wilson, G.J. (1987). Dinoflagellate biostratigraphy of the Cretaceous-Tertiary boundary, mid-Waipara
1337 River Section, North Canterbury, New Zealand. New Zealand Geological Survey Record **20:**
1338 8-16
1339 Witts, J. D., Whittle, R. J., Wignall, P. B., Crame, J. A., Francis, J. E., Newton, R. J. and Bowman, V.
1340 C. (2016) Macrofossil evidence for a rapid and severe Cretaceous–Paleogene mass
1341 extinction in Antarctica. *Nature Communications* **7**, doi:10.1038/ncomms11738.
1342 Zachos, J. C. and Arthur, M. A. (1986). Paleoceanography of Cretaceous/Tertiary boundary
1343 event: Inferences from stable isotopic and other data. *Paleoceanography* **1**: 5-26.
1344 Zachos, J. C., Arthur, M. A. and Dean, W. E. (1989). Geochemical evidence for suppression of
1345 pelagic marine productivity at the Cretaceous/Tertiary boundary. *Nature* **337:** 61-64
1346 Zachos, J. C., Schouten, S., Bohaty, S., Quattlebaum, T., Sluijs, A., Brinkhuis, H., Gibbs, S. J.,
1347 Bralower, T. J. (2006). Extreme warming of mid-latitude coastal ocean during the Paleocene–
1348 Eocene thermal maximum: inferences from TEX_{86} and isotope data. *Geology* **34:** 737–740.
1349 Zachos, J. C., Dickens, G. R., and Zeebe, R. E. (2008). An early Cenozoic perspective on
1350 greenhouse warming and carbon-cycle dynamics. *Nature* **451**: 279-283.
1351 Zhang, Y. G., Pagani, M., and Wang, Z. (2016). Ring Index: A new strategy to evaluate the integrity of
1352 TEX_{86} paleothermometry. *Paleoceanography* **31(2):** 220-232